Natural Resources Canada | Ressources naturelles Canada

GEOLOGICAL SURVEY OF CANADA
OPEN FILE 8491

Forward stratigraphic modelling of a deglacial delta: case study of the Moisie River delta, Quebec

J. Nagle, A. Normandeau, and P. Dietrich

2019

Canada

GEOLOGICAL SURVEY OF CANADA
OPEN FILE 8491

Forward stratigraphic modelling of a deglacial delta: case study of the Moisie River delta, Quebec

J. Nagle[1], A. Normandeau[2], and P. Dietrich[3]

[1] Department of Geology, St. Mary's University, 923 Robbie Street, Halifax, Nova Scotia B3H 3C3
[2] Geological Survey of Canada, 1 Challenger Drive, Dartmouth, Nova Scotia B2Y 4A2
[3] Department of Geology, Auckland Park Kingsway Campus, University of Johannesburg, Johannesburg, South Africa

2019

Permanent link: https://doi.org/10.4095/313665

This publication is available for free download through GEOSCAN (http://geoscan.nrcan.gc.ca/).

Recommended citation
Nagle, J., Normandeau, A., and Dietrich, P., 2019. Forward stratigraphic modelling of a deglacial delta: case study of the Moisie River delta, Quebec; Geological Survey of Canada, Open File 8491, https://doi.org/10.4095/313665

Publications in this series have not been edited; they are released as submitted by the author.

Table of contents

List of figures

List of Tables

Introduction

The controls over deltaic progradation and activity depend on tectonics, sea-level and sediment supply (Bouma, 2004). Recently, studies have shown that in high-latitude regions, glacial erosion and its subsequent sediment transport to the ocean is the main control over deltaic process (Dietrich et al., 2016; Normandeau et al., 2017). Therefore, the recognition of glaciofluvial processes in the stratigraphic record can allow for the reconstruction of ice-margin retreat (Dietrich et al., 2017).

In remote Arctic regions, the reconstruction of deltaic activity is limited by the rarity of samples and dated material. However, when the main controls over deltaic activity are known, modelling can become a valuable tool for the reconstruction of deltaic progradation and starvation. In order to evaluate the usefulness of forward stratigraphic modelling, the goal of this study was to validate the model of progradation of a delta in an undammed fjord of Dietrich et al. (2017) by studying the well-known Moisie River delta (Dietrich et al., 2018; Dubois, 1979; Lessard and Dubois, 1984; Normandeau et al., 2013). On the Moisie River delta, late deglaciation of the watershed occurred, which caused glaciofluvial delta progradation during falling relative sea level. Sediment supply to the deltas ceased when the ice-margin retreated from the watershed.

Regional settings

The study area is located in Sept-Îles, along the Québec North Shore (Fig. 1). Here, a large deltaic complex was formed during deglaciation. Today, the delta is about 13 km long and 33 km wide, indicating that longshore processes were a prime control over the present-day morphology.

Glacial retreat in the area began at ~11 ka BP, with the ice-margin retreating from the watershed at ~7.3 ka BP (Dietrich et al., 2017). During the first 3.7 ka of glacial retreat, the watershed was supplied with a large quantity of glacial meltwater, which loaded the river with sediments, causing glaciofluvial progradation of the delta. Starting at approximately 7.3 ka BP, the glacier retreated from the watershed, cutting off the supply of sediment and meltwater. This essentially caused the delta to stop prograding, and to switch to a wave-dominated delta. During the last 7.3 ka, it is interpreted that the delta has been modified mainly by longshore drift, causing it to erode in the east, and accrete in the west.

Methods

For the purpose of this study, the 2017 version of DionisosFlow was used since this version has the ability to model longshore drift, an important component of deltaic evolution. DionisosFlow is a 3D forward stratigraphic modelling software that allows for the reconstruction of regional and basin scale processes (Bruneau et al., 2018). It can perform these processes over geological time scales (Granjeon et al., 2014). The software relies on diffusion principles, which allows the sediment grain to be affected by multiple transportation mechanisms. With this data, mass balance equations are applied and the net product of sediment supply, transportation, subsidence, sea level fluctuation, and uplift can be calculated at each time step (Granjeon et al., 2014). This data is then represented as a 4D model.

The evolution of the Sept-Îles deltaic complex occurred on an 11 ka time scale. To avoid problems with using too small of a time step in DionisosFlow, the age of the deltaic complex was multiplied by 1000, total sediment supply was divided by 1000, and total fluvial discharge was divided by 100 (Dietrich, 2015). This allowed the model to function on an 11 Ma time scale. This step was required by the software since it generally deals with sequences spanning millions of years.

Calibration of the Model

In order to check the reliability of the model, it has to be calibrated. The first step in the calibration process is comparing the model to the present day morphology of the delta. A thickness map as well as high resolution LiDAR images were used. The initial topography (Fig. 2) that the model used was constructed from the terrestrial and bathymetry DEM with the known sediment thickness removed. The initial topography thus assumes that no sediment is present on land or under water prior to delta progradation. Two models are presented in this study, which have very limited differences.

Parameters Used in Model 1.

Most of the values used within the modelled delta are from Dietrich (2015) for a similar delta on the St. Lawrence Estuary, realizing that some of these values may not be realistic for our modelled delta. The bedrock coefficient values have been altered due to errors that arose when trying to increase the resolution. The influence of bedrock on the modelled environment is considered to be

insignificant due to the 11 ka time span. Model 1 ran at a 500 year time step. Below is a summary of each parameter used within the DionisosFlow software:

Domain

The domain of the study area is 100 km x 140 km with the bounding box starting point at X_0 = -7420 km and Y_0 = 6360 km. This has been broken up into 56,000 cells, each measuring 500 m x 500 m.

Sediment Classes and Properties

The granulometries present in the deltaic complex consist of clay, sand, and bedrock. The clay fraction has a grain size of 0.002 mm, the sand fraction has a grain size of 1 mm, and the bedrock was set to a grain size of 1000 mm. All three sediment types have the same density of 2500 kg/m^3.

Structural Evolution

The initial substratum consists of bedrock that is 1 m thick. There is no subsidence or flexure.

Eustasy

The eustasy curve is from Dietrich et al. (2017) and has been modified to have a starting sea level of 132 m at 11 ka (Fig. 3).

Sediment Supply

One river was used to supply the Sept Îles deltaic complex. It had a sediment load that consisted of 67 % sand and 33 % clay, and was 2000 m wide. Sedimentation was considered to be constant per each time interval. Rainfall and evaporation were not taken into account. Table 1 shows the values used for total sediment supply and total fluvial discharge for each time step. The computational parameters consisted of 155 km^3/Ma for sediment supply, 100 m^3/s for fluvial discharge, and 0.098 kg/m^3 for concentration.

Transport Processes

Transport processes are what control sediment behaviour. The Linear Diffusive Transport Law was used, and channelized force was set to zero. Channelized force refers to a computation mode for water flow. Setting this to zero causes water flow to act like a homogenized sheet that is distributed, whereas setting this to one causes the water flow to be random with a unique channel (OpenFlow Suite 2017.1). For low energy long term (LELT) transport, the average continental depositional slope was set to 5 m/km and the average marine depositional slope was set to 8 m/km.

LELT transport is always active in the modelled environment. It takes into account gravity processes (slumping, etc.) and transport due to water processes (rivers) (OpenFlow Suite 2017.1). The ratio between gravity and water processes was set to 12, meaning that it favors water driven transport more than gravity driven transport. The Slope Failure Model was performed using the Gravity Friction Model, with the basement always stable, and debris mode set to one block. The Erosion Model was set to maximum weathering rate for each sediment utilizing the Arithmetic Mixing Law, with the maximum decay in marine environments set to 10 m. The transport parameters for each sediment is located in Table 2.

Waves Impact

Two types of waves were modelled to take into account ocean processes. The first type of waves had a wave base of 10 m, a wave propagation azimuth of 280˚, and occurred 100% throughout the year. The second type of waves had a wave base of 30 m, a wave propagation azimuth of 280˚, and occurred 10% throughout the year. The first type of wave represented the normal wave influence that occurred in the St. Lawrence, whereas the second type of waves represented storms. These waves occurred throughout the 11 ka time span.

Ocean properties, climatic properties, and carbonate production were not accounted for in this study.

Parameters Used in Model 2

The values used in Model 2 are very similar to Model 1. The only difference is that it ran at a lesser resolution (larger cell size 1250 m x 1250 m), and at a finer time step (100 years). The values used in the Sediment Supply Editor and the Transport Editor for Model 2 are in Tables 3 and 4 respectively.

Results

Model 1

The evolution of delta progradation of model 1 is illustrated in figures 4-19. Delta progradation begins at 10.5 ka BP (Figs. 4, 12) when the glacier is providing the watershed with abundant meltwater and recently eroded sediment. This allows for delta foresets to develop. Marine terraces start to form at 9.5 ka BP (Figs. 4, 12) and submarine channels formed at 10 ka BP (Fig. 12). As delta progradation continues, sea level is drastically lowering. This allows the delta to prograde to

a maximum extent at 7 ka BP (Figs 6, 14). After the ice margin left the watershed, the delta appears to continue prograding (Fig. 15), however, it could be an artifact of sea level lowering. Once the river flow has decreased, the delta begins to be eroded by waves and longshore drift. Submarine channel flow appears to diminish to a very low rate. This occurs at approximately 7 ka BP (Figs. 6-11, 14-19). Another marine terrace formed at 5 ka BP. At present day (0 Ka), the delta appears to have multiple marine terraces and a large river incision towards the right side of the delta. It also appears to be 110 m thick (Fig. 20, *see* Fig. 36A). When looking at Figure 20, the delta appears to have been eroded by waves from 8 ka to present. This contributed to the movement of sands deep into the basin as seen in time step 0.

Model 2

Model 2 has a similar development as Model 1 (Figs. 21-36). Delta progradation begins at 10.9 ka BP. This is because the model ran at a smaller time step (100 years), allowing it to show more detail. At 10.5 ka BP (Figs. 21, 29) the delta has developed foresets (Fig. 37). Marine terraces start to form at 9 ka BP (Figs. 22, 30). Sediment input from glacial meltwater and sea level drastically lowering, allowed the delta to prograde until ~7 ka BP (Figs. 23, 31). Once the glacier left the watershed, wave-dominated sedimentation processes occur. Erosion from wave action and longshore drift caused the delta to migrate towards the west. Fluvial incision of the delta appears to have occurred at 5.5 ka BP (Fig. 32). Another marine terrace formed by 6 ka BP (Figs. 24, 32). Delta progradation continued until 5 ka due to sea level fall (Fig. 32). Today, the delta has developed multiple marine terraces, with river incision occurring towards the western side of the delta, which is approximately 120-130 m thick (Fig. 38). When looking at the cross section (Fig. 37), the delta has developed river incision, which caused the formation of a marine terrace at 4 ka BP. The erosion of the delta also pushed sands deep into the basin as seen in time step 0 (Fig. 36).

Discussion

Morphological comparison between the model and the Moisie River delta

The final morphology of the models is reasonably consistent with the present-day Moisie River delta. Both Models 1 and 2 resulted in a ca. 40 km wide, 20 km long delta (Fig. 38). These measurements are reasonably close to the 33 km wide, 13 km long delta. The differences in length are most likely due to the lower erosion rates in the models compared to the real delta. Indeed, the Moisie River delta is a wave-dominated delta that has been eroded and its morphology reflects

strong east to west longshore drift. Although the models show some influence of longshore drift, it did not produce enough wave-action erosion consistent with the present-day morphology. These lower erosion rates in the model outputs are probably responsible for the longer delta than the present-day one.

The thickness maps also share very similar characteristics. The models produced ca. 130 m thick sediment succession whereas the present-day delta is approximately 120-140 m thick. More importantly, the distribution of sediment produced by the models closely matches the present-day delta. The present-day delta constructed the Lake Daigle sandur delta at an elevation of 135 m to the west of the river (Dietrich et al., 2016), which is also observed in the thickness maps of models 1 and 2. The general morphology of the delta and its thickness are thus reasonably well reproduced by the modelling.

Evolution of the Moisie River delta based on the modelling

According to stratigraphic studies, the Moisie River delta began prograding into the Gulf of St. Lawrence at 10.8 ka BP until 7.3 ka BP. The delta was fed by high glaciofluvial sediment supply and relative sea-level was falling rapidly. Despite sea-level fall, the river was not incising the delta plain (Dietrich et al., 2018). At 7.3 ka BP, the ice-margin retreated from the watershed, which drastically diminished sediment supply. Coastal processes therefore began reworking the delta front (Dietrich et al., 2018).

Both models presented are fairly consistent with the present-day Moisie River progradation. According to the models, the delta prograded rapidly between 10.5 and 7 ka BP due to high sediment input into the system. Between 7 ka BP and 5 ka BP, sediment input was greatly reduced, which lowered progradation rates during sea level fall. When the rate of sea-level fall lowered around 5 ka BP, the shoreline became relatively stable, suggesting an equilibrium between sea-level fall and erosion of the shoreline by wave action. Starting at 1.5 ka BP, the shoreline began eroding more quickly and sediment was transferred westward, even though sea-level was still lowering. This erosion during sea level fall shows the influence of the near-absence of sediment supply to deltas on delta erosion. Additionally, the models suggest that sediment supply and the rate of sea-level fall are both important parameters. Sediment supply appears as the dominant parameter during deglaciation. However, when the ice-margin retreats from the watershed, the rate of sea-level fall (not the position of sea-level) becomes an important parameter on delta erosion.

When the rate of sea-level fall lowers, coastal processes become the dominant control over deltaic evolution.

Conclusions

This study aimed at validating a model where variations in sediment supply due to a retreating glacier in combination with a falling sea-level could be reproduced numerically. Stratigraphic forward modelling of the Moisie River delta proved to be effective in reproducing the present-day delta and its evolution. The modelled Holocene evolution of the delta was fairly consistent with the known evolution. When parameters governing deltaic evolution are known, stratigraphic forward modelling appears to be an effective tool to understand past deltaic processes. This approach could be an interesting method for understanding past behaviour of Arctic deltas, where data is limited. In addition, it could help predicting future behaviour of Arctic deltas where glaciers and ice sheets are melting.

Acknowledgements

The authors wish to thank Prof. Georgia Pe-Piper (St. Mary's University) for supporting this project through the use of Dionisos Flow.

References

Bruneau, B., Chauveau, B., Duarte, L.V., Desaubliaux, G., Moretti, I., Baudin, F., 2018. 3D numerical modelling of marine organic matter distribution: example of the early Jurassic sequences of the Lusitanian Basin (Portugal). Basin Res. 30, 101–123.

Dietrich, P., 2015. Faciès, architectures stratigraphiques et dynamiques sédimentaires en contexte de régression forcée glacio-isostatique (Thesis). École Dr. des Sci. la terre l'environnement. Université de Strasbourg, Strasbourg.

Dietrich, P., Ghienne, J., Lajeunesse, P., Normandeau, A., Deschamps, R., Razin, P., Scotia, N., Bordeaux, I.P. De, 2018. Deglacial sequences and glacio-isostatic adjustment : Quaternary compared with Ordovician glaciations.

Dietrich, P., Ghienne, J.-F., Normandeau, A., Lajeunesse, P., 2017. Reconstructing ice-margin retreat using delta morphostratigraphy. Sci. Rep. 7, 16936. doi:10.1038/s41598-017-16763-x

Dietrich, P., Ghienne, J.-F., Schuster, M., Lajeunesse, P., Nutz, A., Deschamps, R., Roquin, C., Duringer, P., 2016. From outwash to coastal systems in the Portneuf-Forestville deltaic complex (Québec North Shore): Anatomy of a forced regressive deglacial sequence. Sedimentology. doi:10.1111/sed.12340

Dionne, J.-C., 2001. Relative sea-level changes in the St. Lawrence estuary from deglaciation to present day, in: Weddle, T.K., Retelle, M.J. (Eds.), Deglacial History and Relative Sea-Level Changes, Northern New England and Adjacent Canada. Geological Society of America Special Paper, Boulder, Colorado, pp. 271–284.

Dubois, J.-M., 1979. Environnement quaternaire et évolution post-glaciaire d'une zone côtière en émersion en bordure sud du Bouclier Canadien: la Moyenne Côte-Nord du Saint-Laurent, Québec (Thesis). Département de Géographie. Université d'Ottawa.

Granjeon, D., Martinius, A.W., Ravnas, R., Howell, J.A., Steel, R.J., Wonham, J.P., 2014. 3D forward modelling of the impact of sediment transport and base level cycles on continental margins and incised valleys. Depos. Syst. to Sediment. Successions Nor. Cont. Margin Int. Assoc. Sedimentol. Spec. Publ. 46, 453–472.

Lessard, G.L., Dubois, J.-M.M., 1984. Évolution littorale multitemporelle d'une côte récemment déglacée du nord du gole du Saint-Laurent. Rev. géomorphologie Dyn. 33, 81–96.

Normandeau, A., Dietrich, P., Lajeunesse, P., St-onge, G., Ghienne, J., Duchesne, M.J., Francus, P., 2017. Timing and controls on the delivery of coarse sediment to deltas and submarine fans on a formerly glaciated coast and shelf. GSA Bull. 129, 1424–1441. doi:10.1130/B31678.1

Normandeau, A., Lajeunesse, P., St-Onge, G., 2013. Shallow-water longshore drift-fed submarine fan deposition (Moisie River Delta, Eastern Canada). Geo-Marine Lett. 33, 391–403. doi:10.1007/s00367-013-0336-0

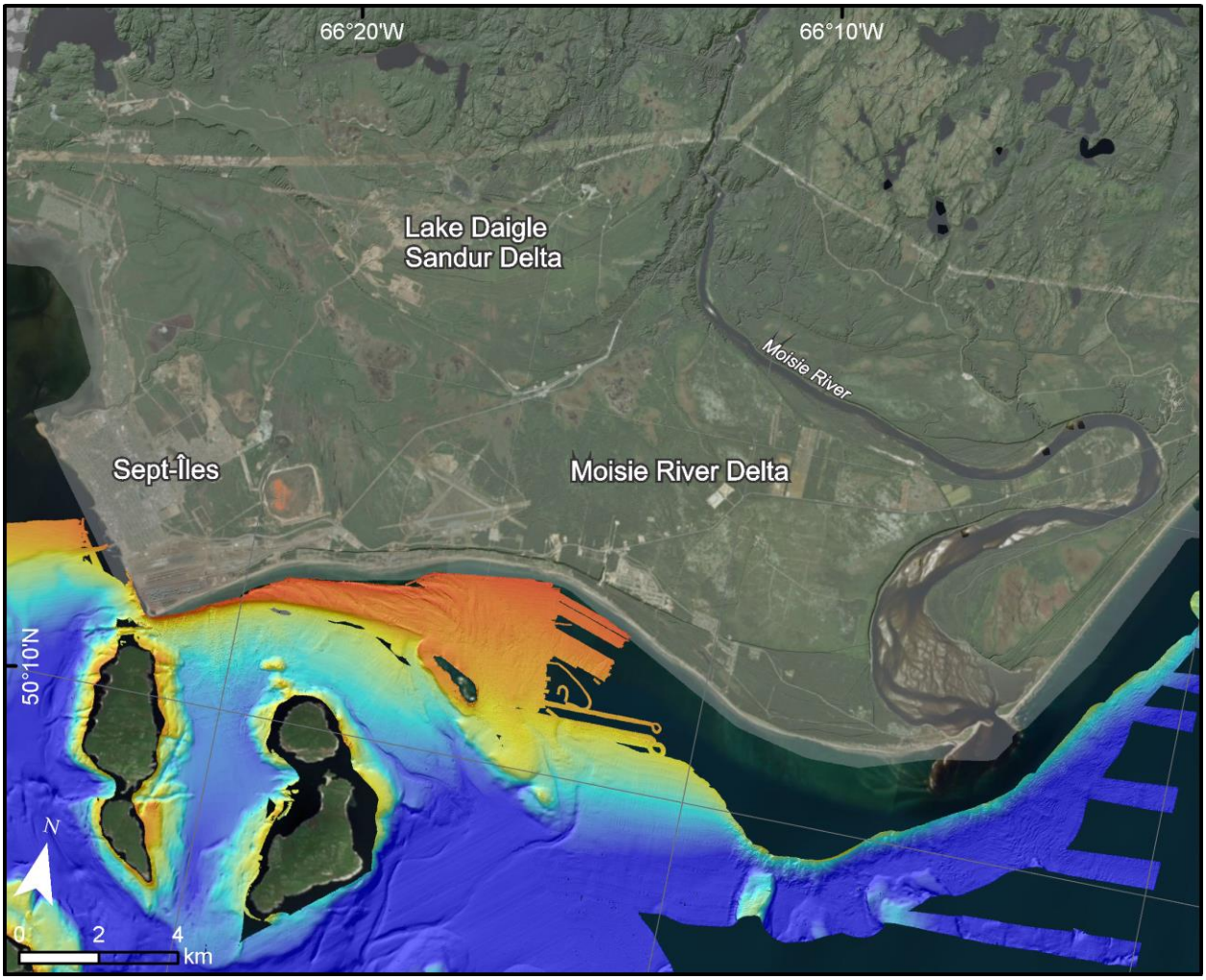

Figure 1: Present day view of the Sept-Îles deltaic complex.

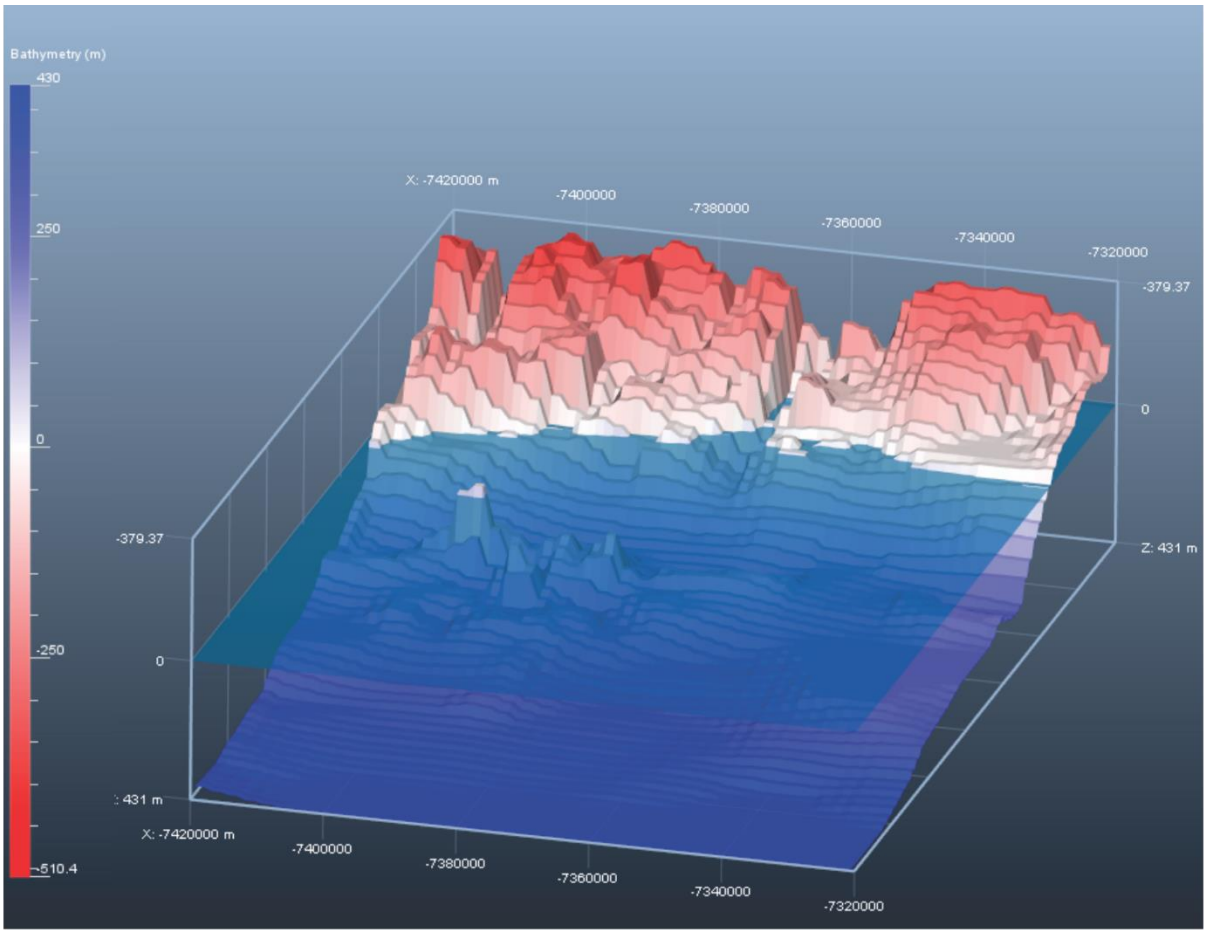

Figure 2: Processed bathymetric map showing the starting topography and sea level at 11 Ka.

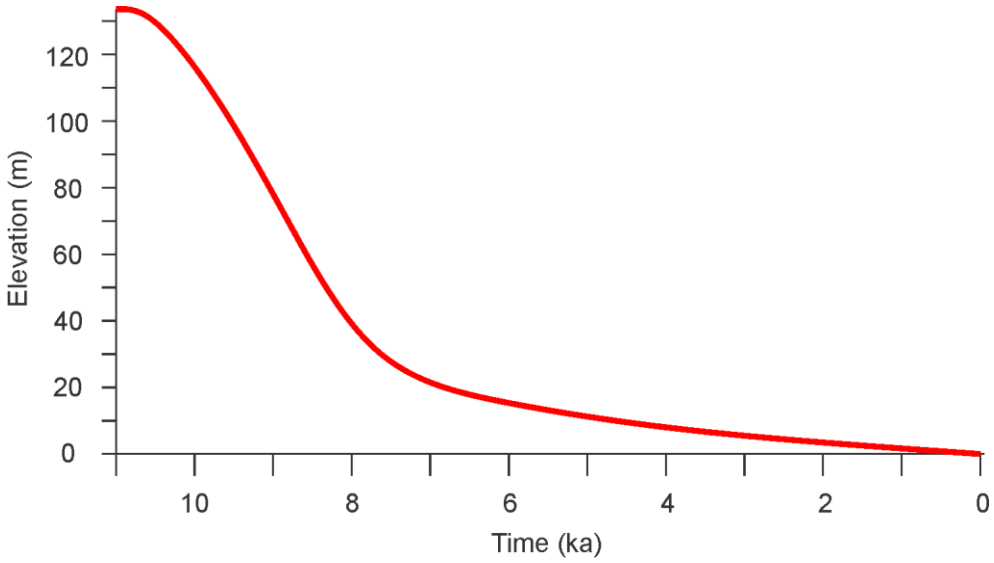

Figure 3: Relative sea level fall diagram (modified from Dietrich et al. 2017).

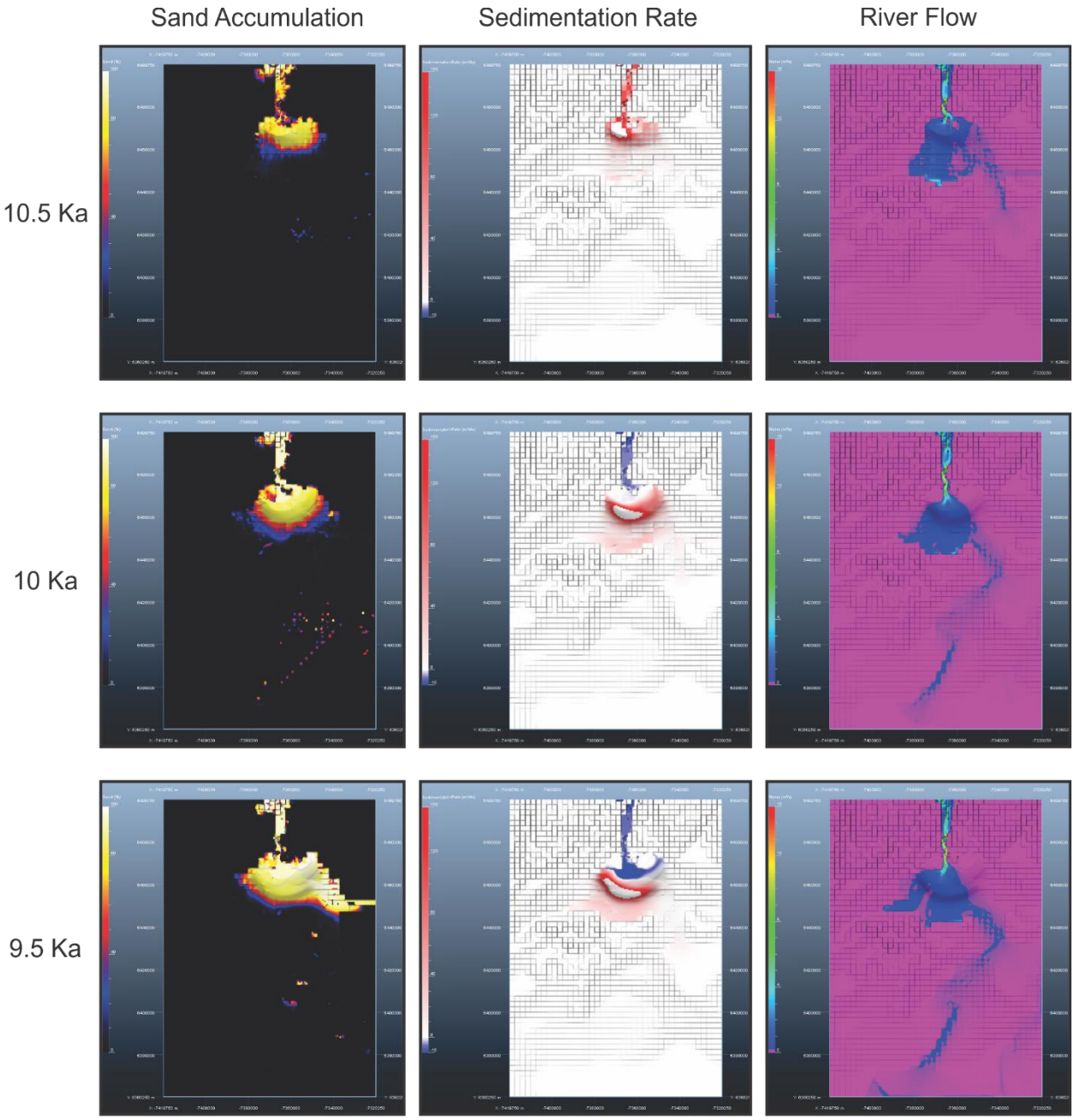

Figure 4: Plan view of delta progradation for Model 1 from 10.5 ka BP to 9.5 ka BP

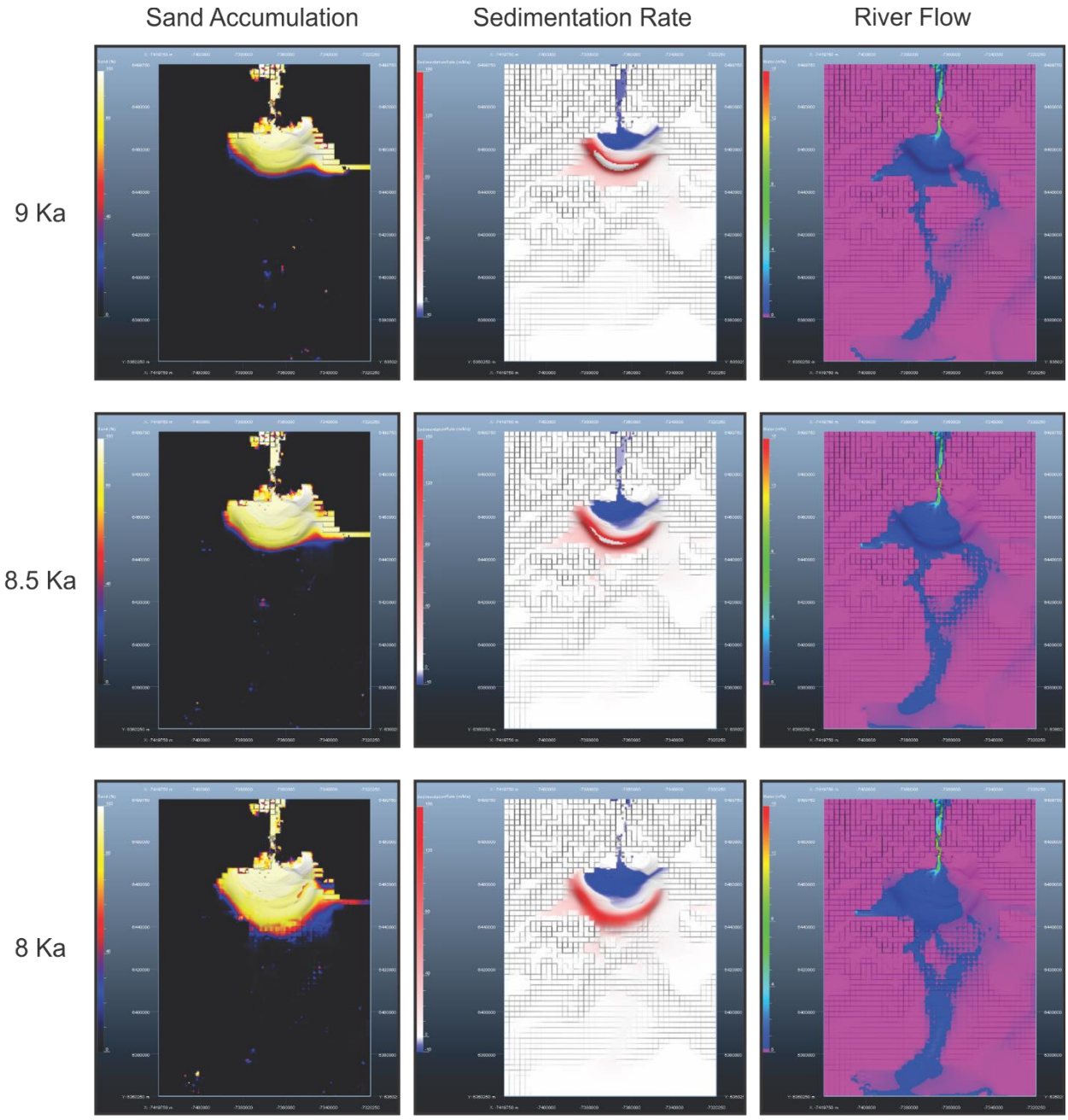

Figure 5: Plan view of delta progradation for Model 1 from 9 ka BP to 8 ka BP.

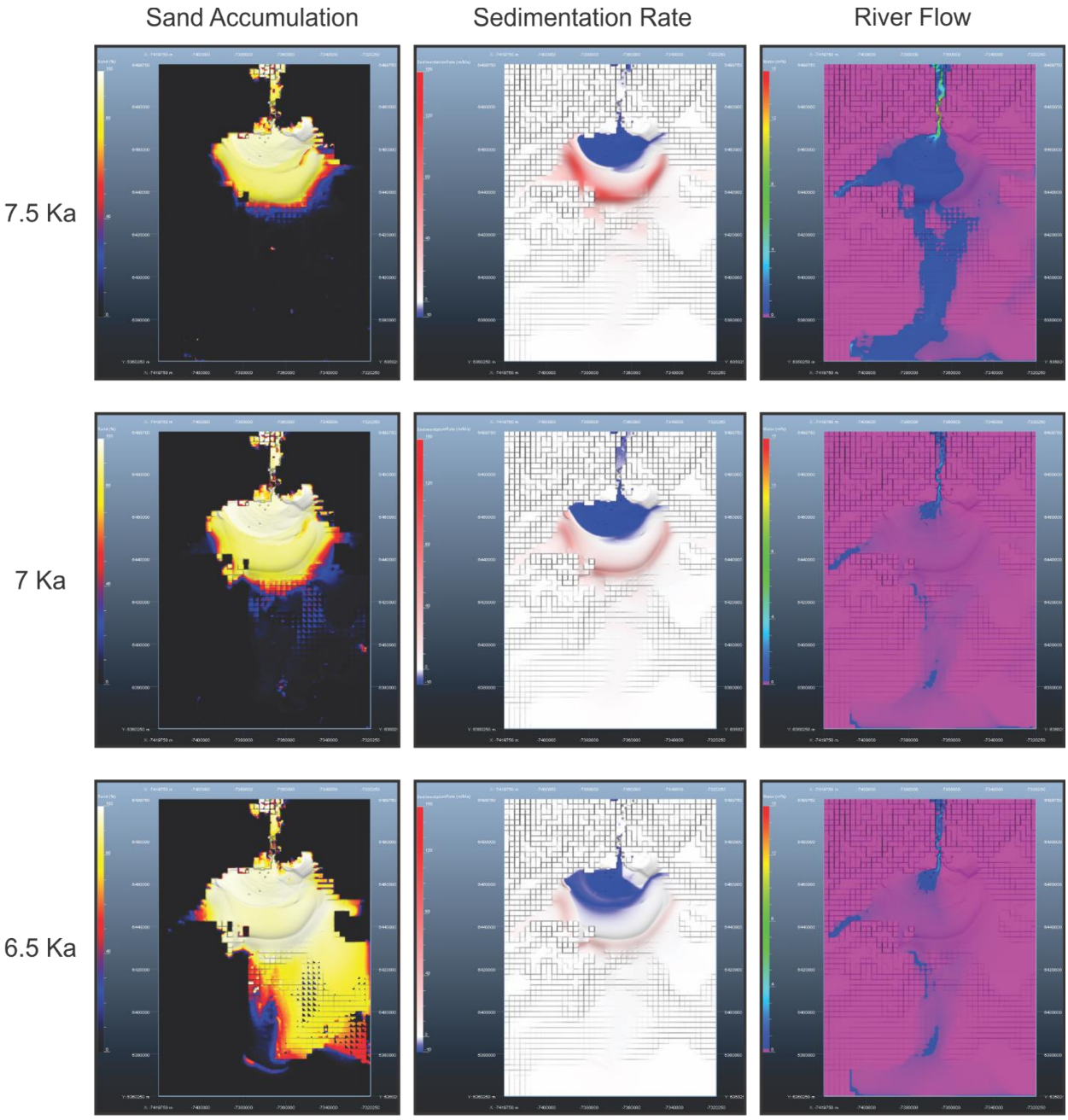

Figure 6: Plan view of delta progradation for Model 1 from 7.5 ka BP to 6.5 ka BP

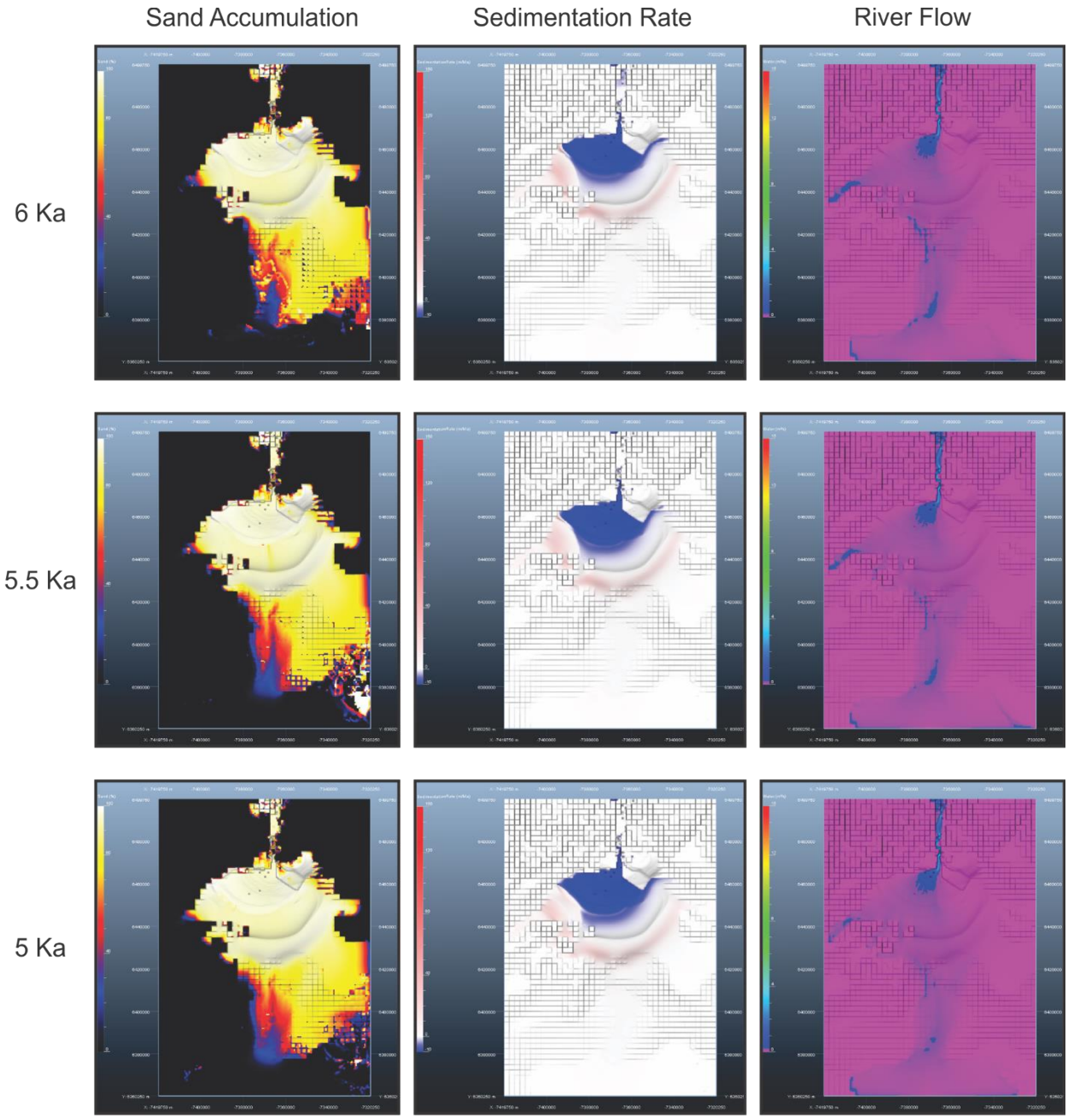

Figure 7: Plan view of delta progradation for Model 1 from 6 ka BP to 5 ka BP

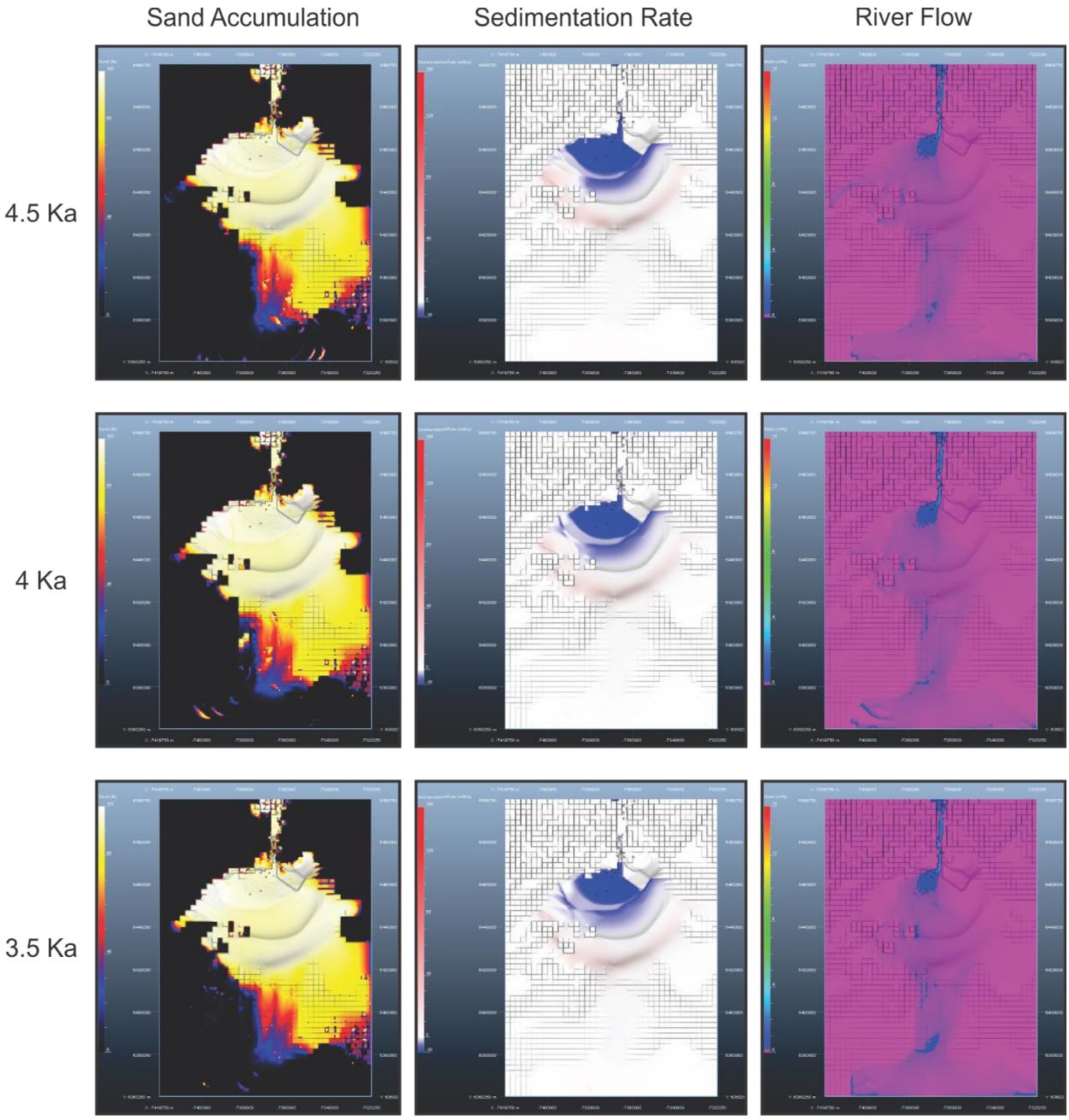

Figure 8: Plan view of delta progradation for Model 1 from 4.5 ka BP to 3.5 ka BP

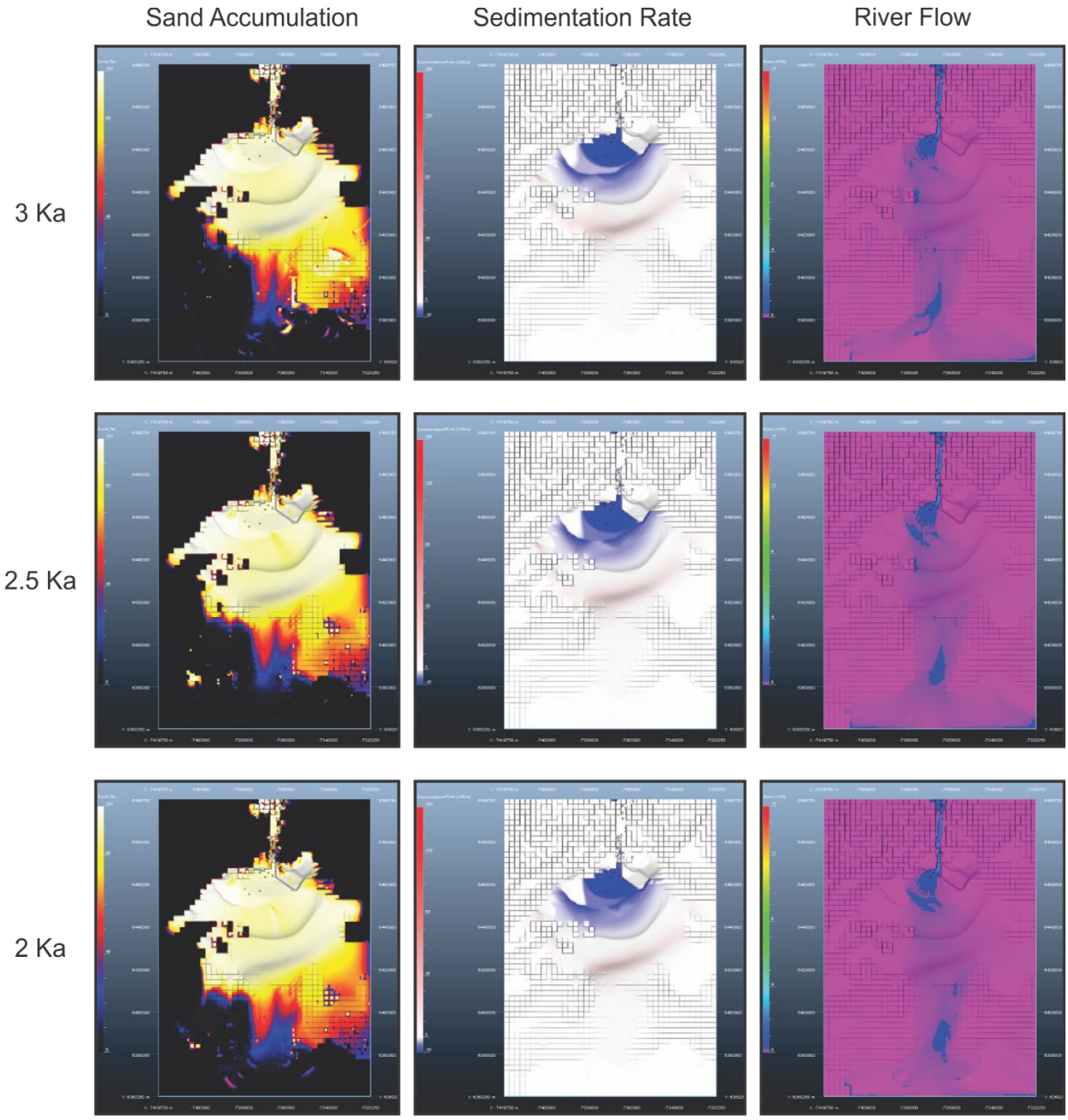

Figure 9: Plan view of delta progradation for Model 1 from 3 ka BP to 2 ka BP

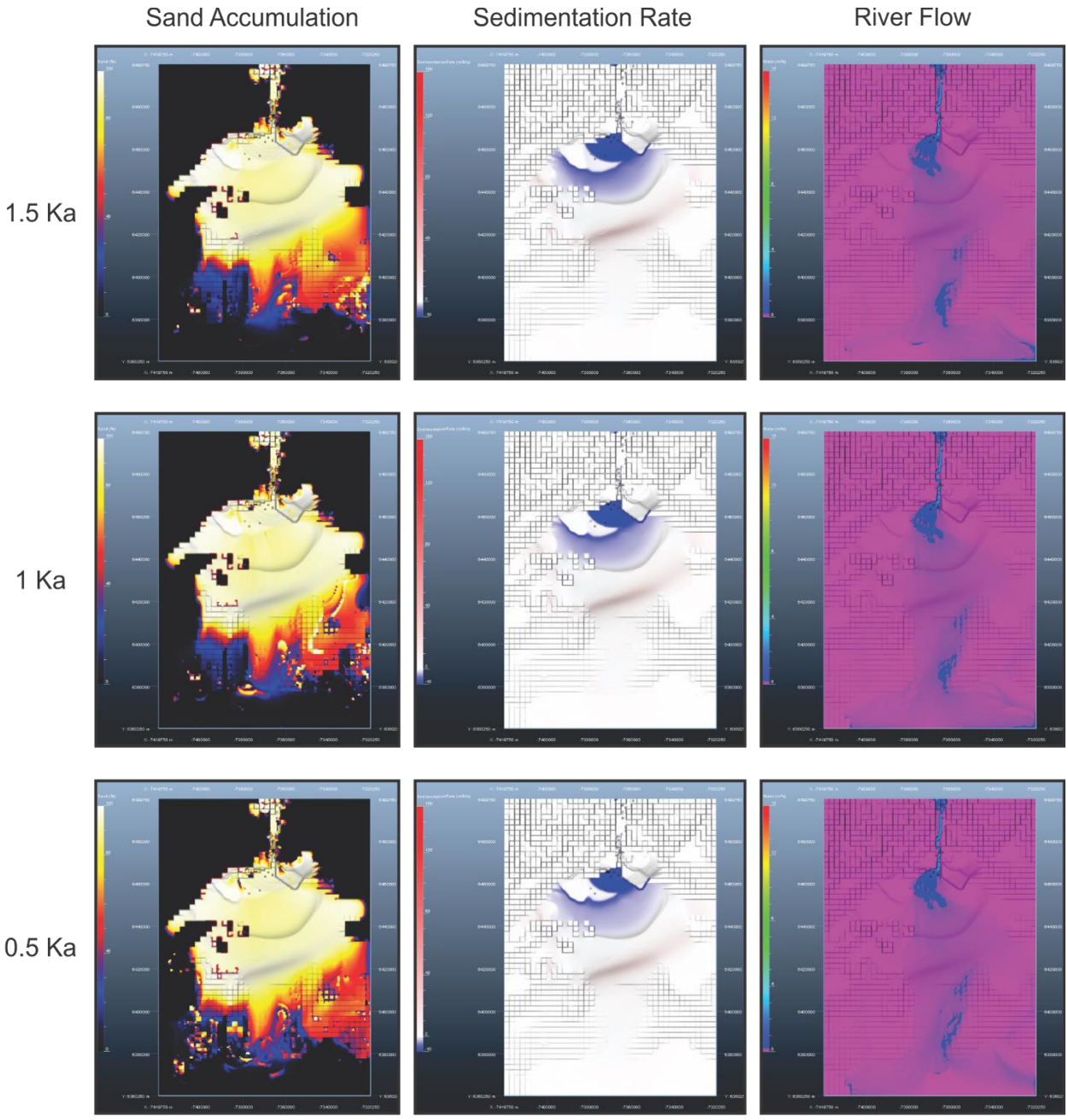

Figure 10: Plan view of delta progradation for Model 1 from 0.5 ka BP to 1.5 ka BP

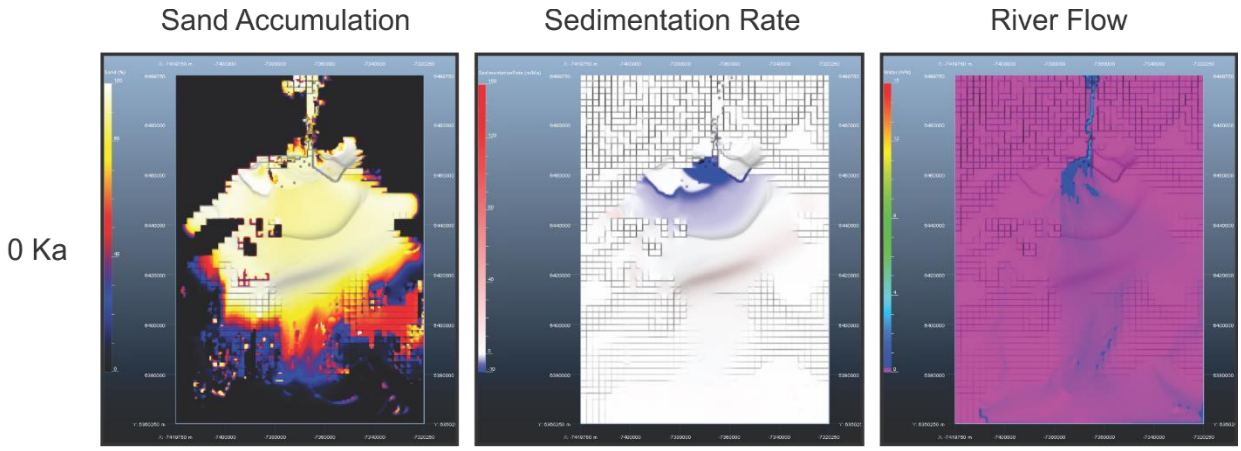

Figure 11: Plan view of delta progradation for Model 1 at present day.

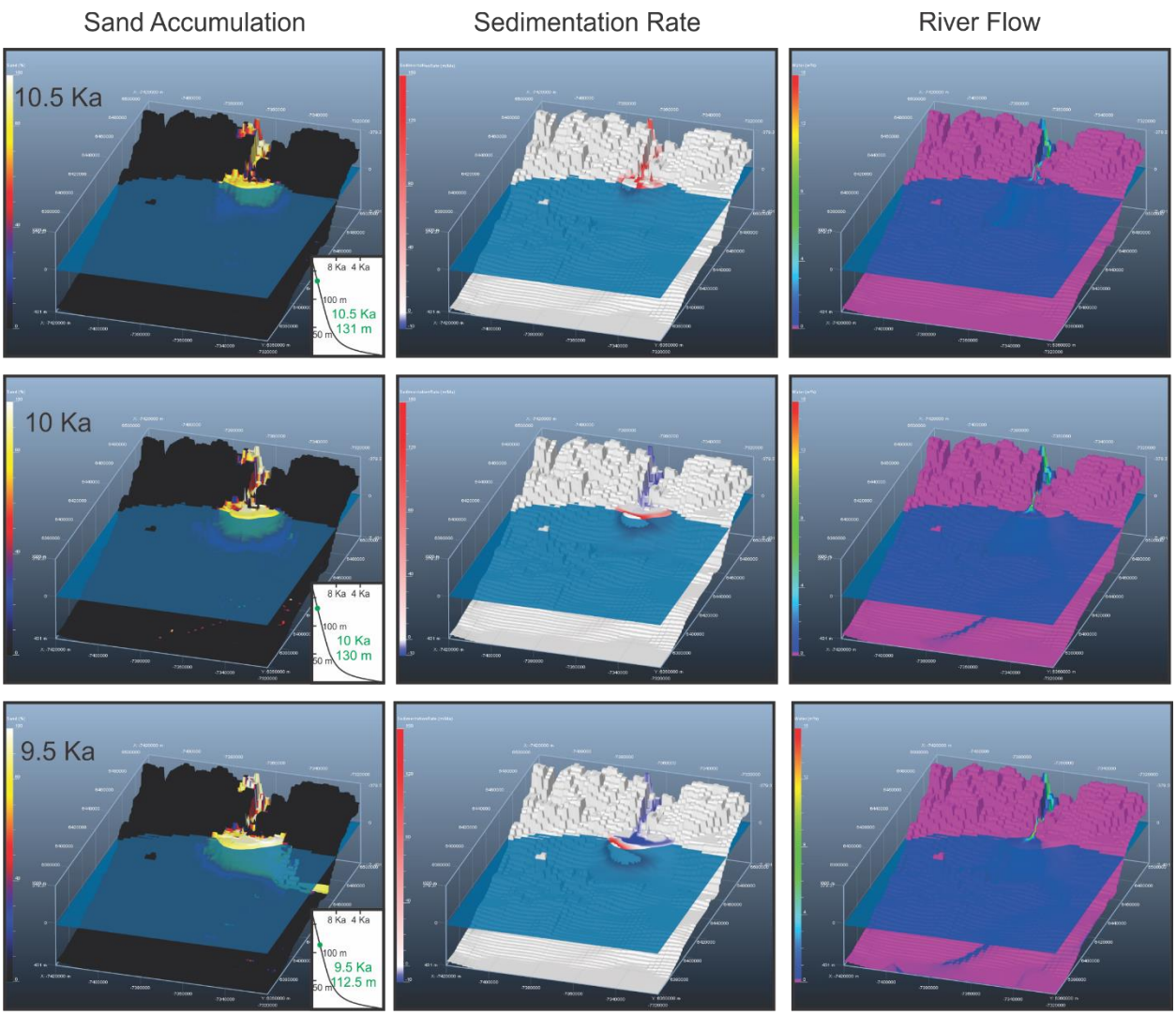

Figure 12: 3D view of Model 1 from 10.5 ka BP to 9.5 ka BP.

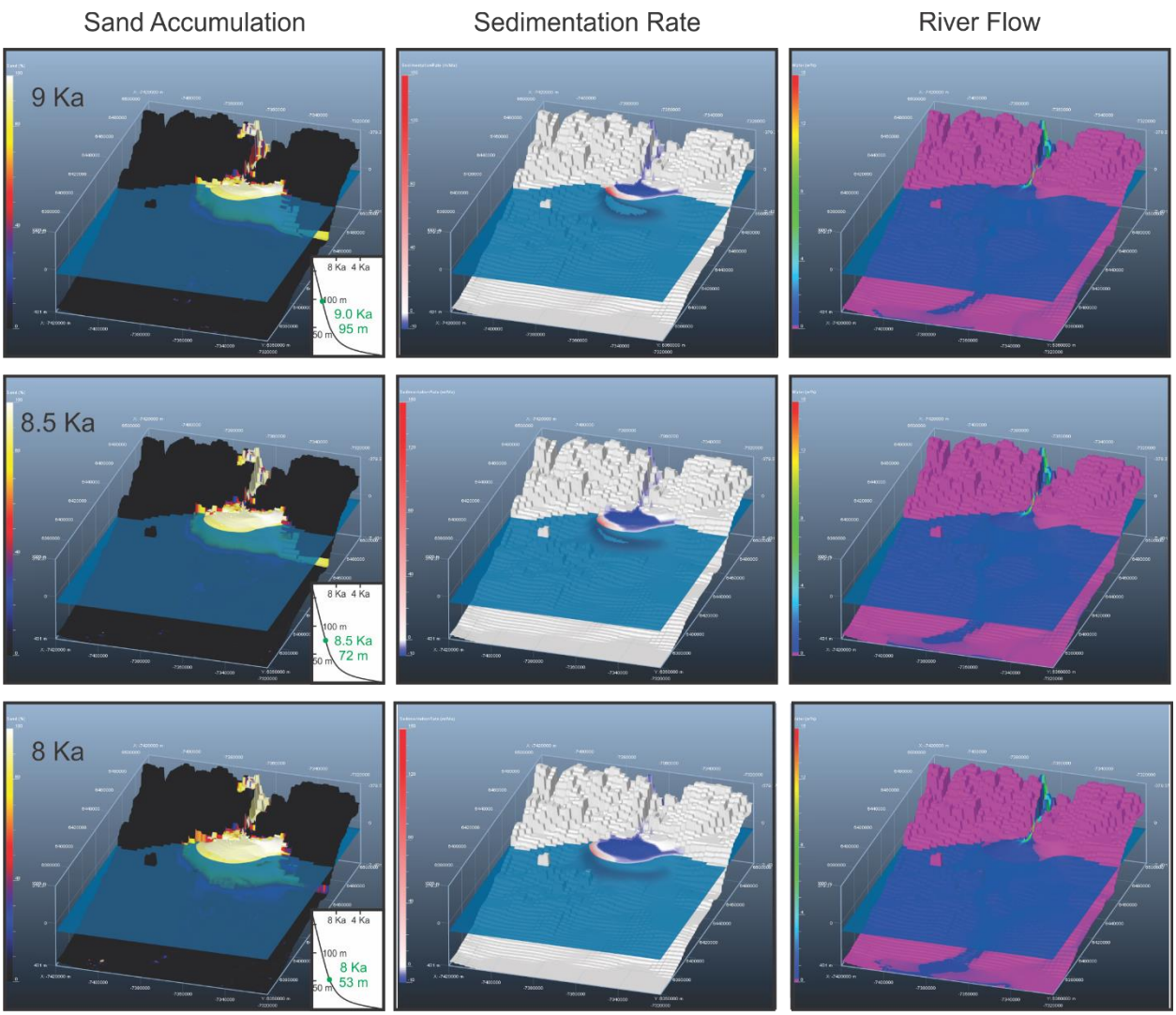

Figure 13: 3D view of Model 1 from 9 ka BP to 8 ka BP.

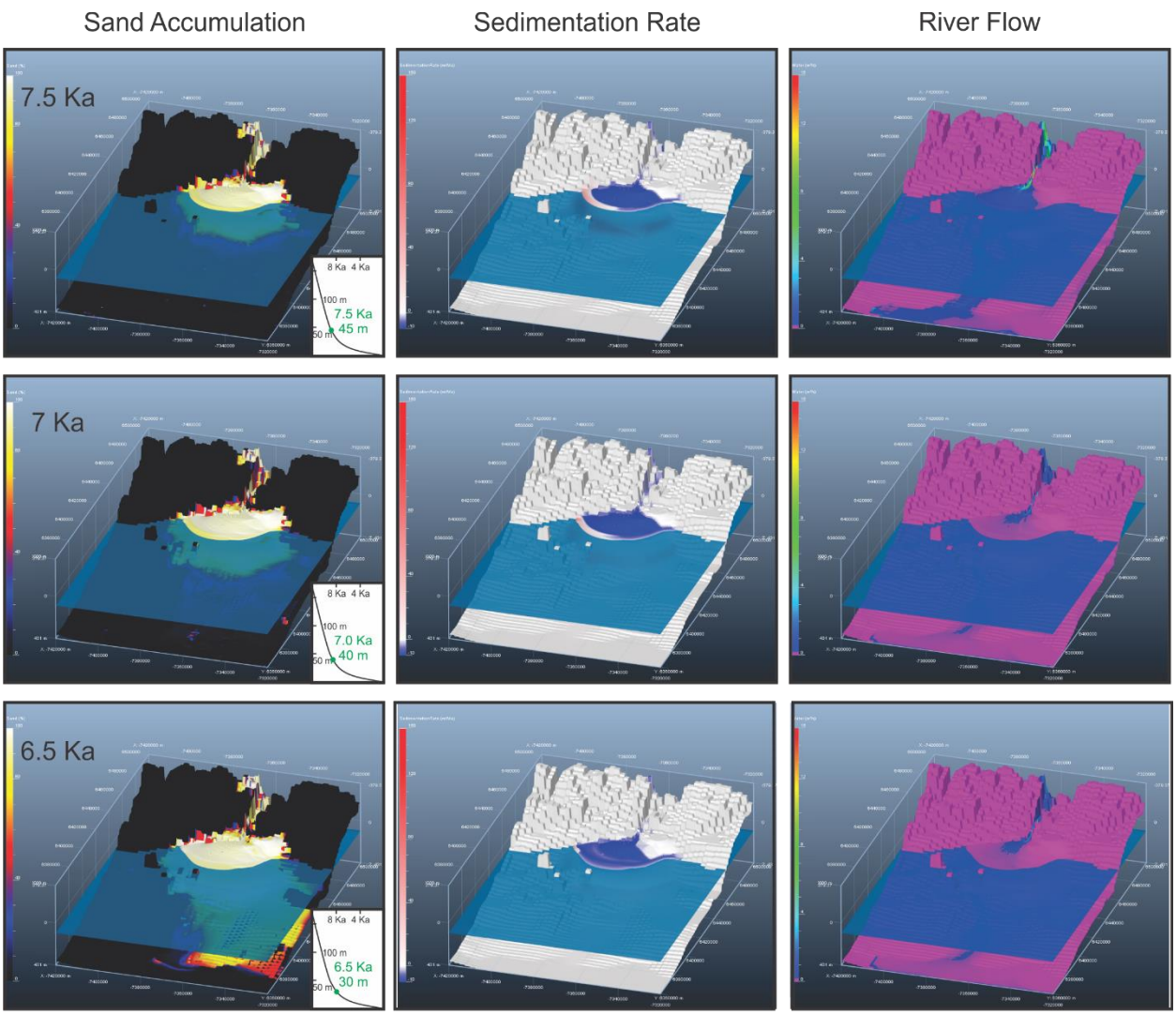

Figure 14: 3D view of Model 1 from 8.5 ka BP to 6.5 ka BP.

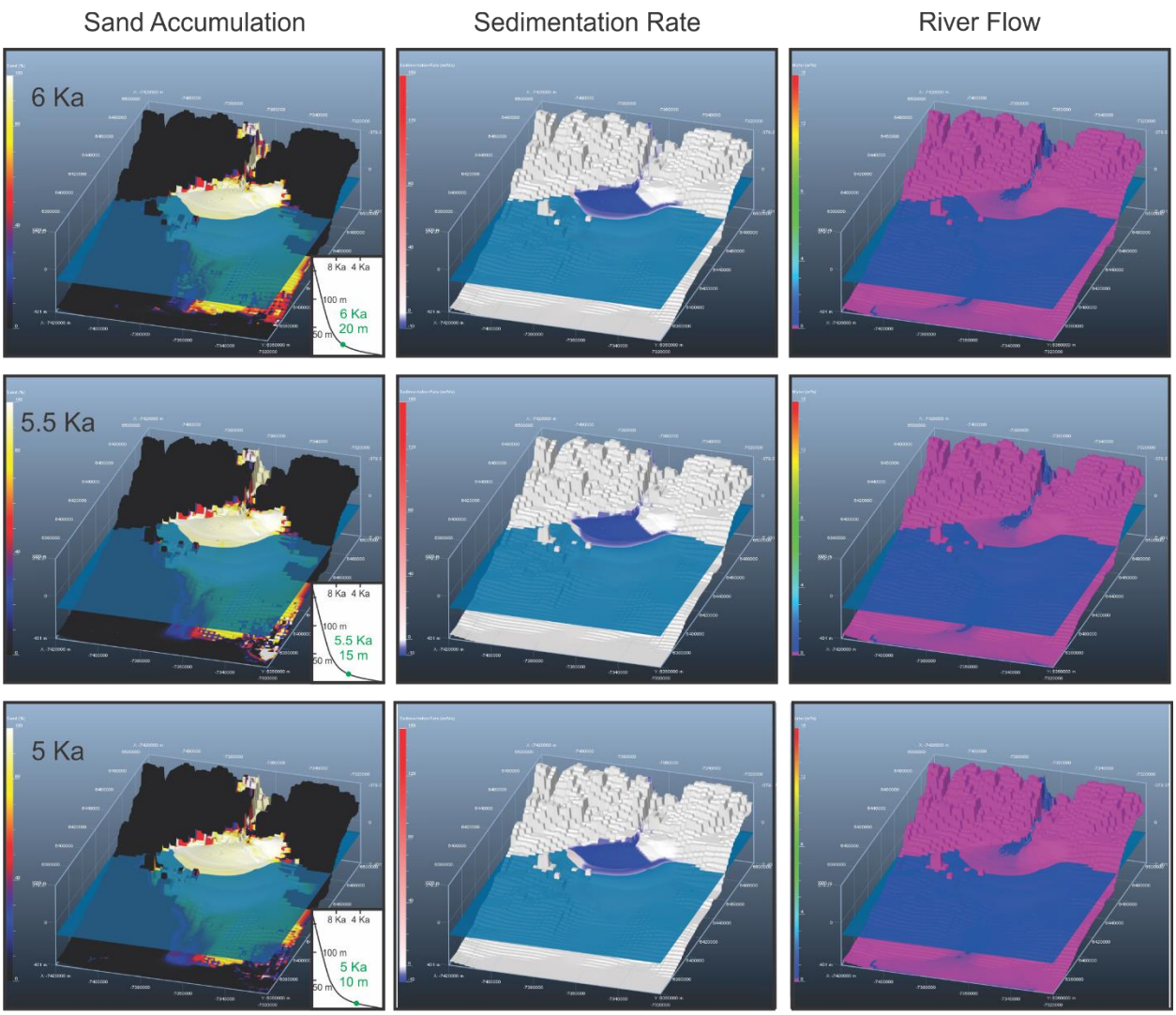

Figure 15: 3D view of Model 1 from 6 ka BP to 5 ka BP.

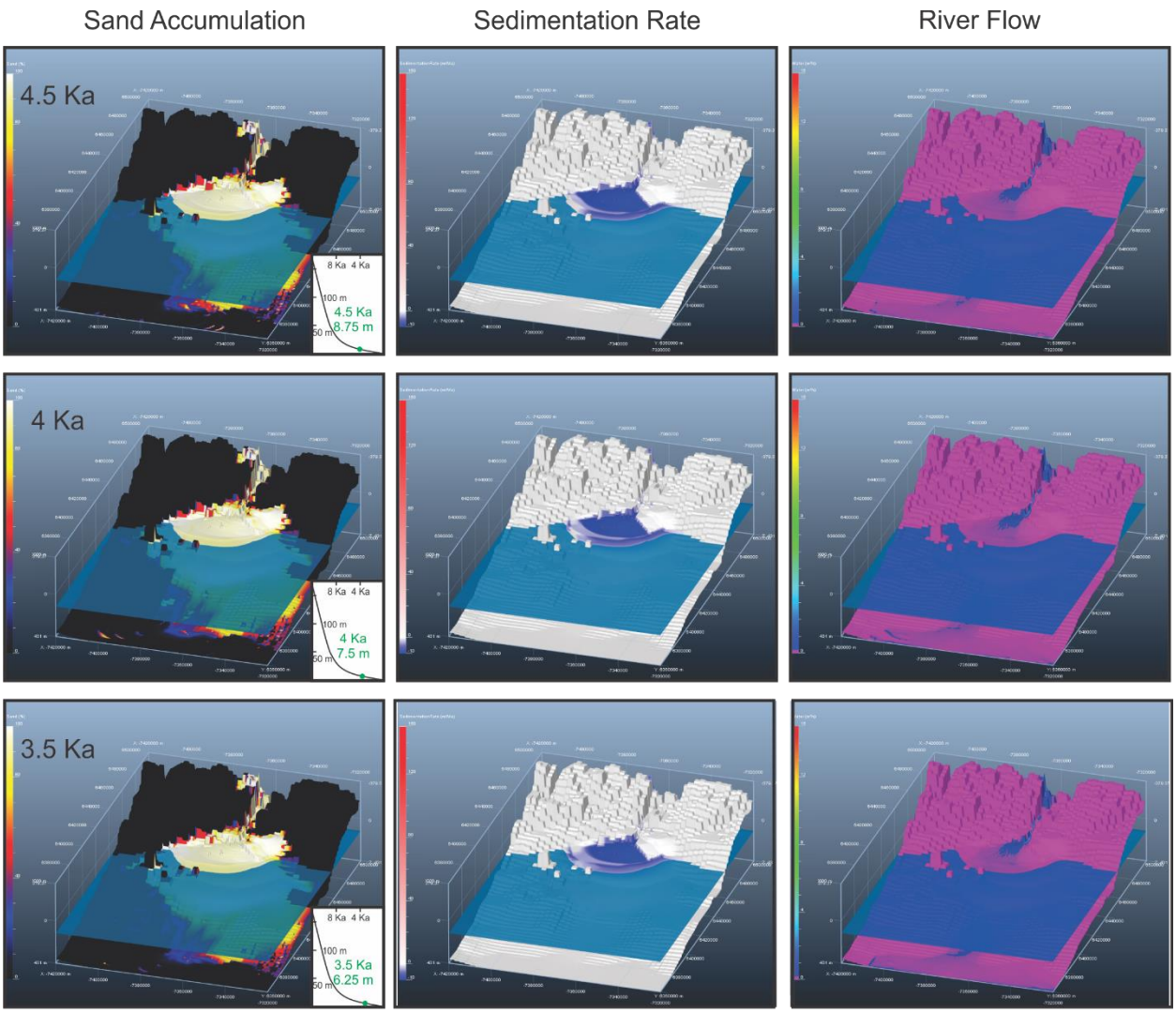

Figure 16: 3D view of Model 1 from 3.5 ka BP to 4.5 ka BP.

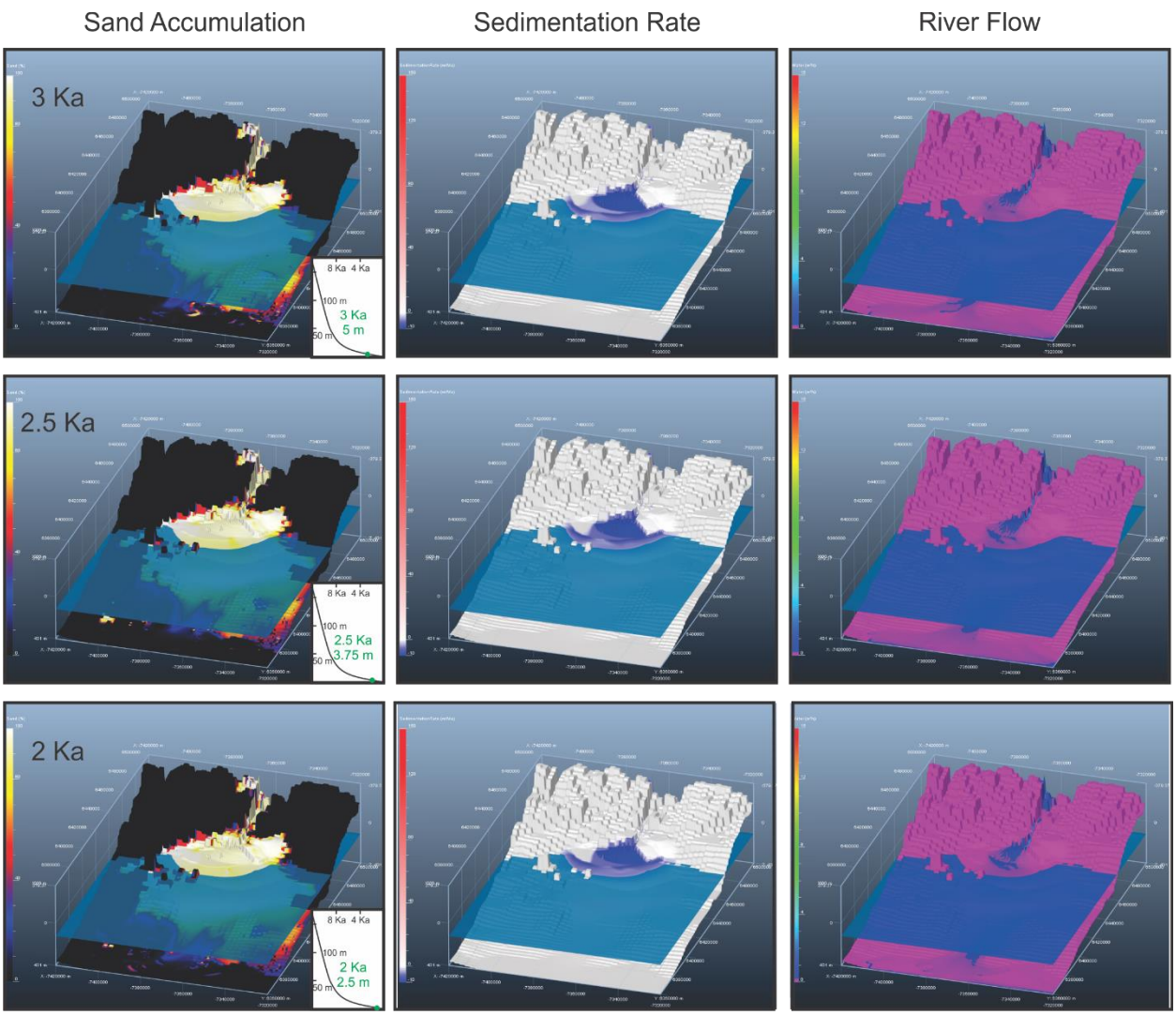

Figure 17: 3D view of Model 1 from 3 ka BP to 2 ka BP.

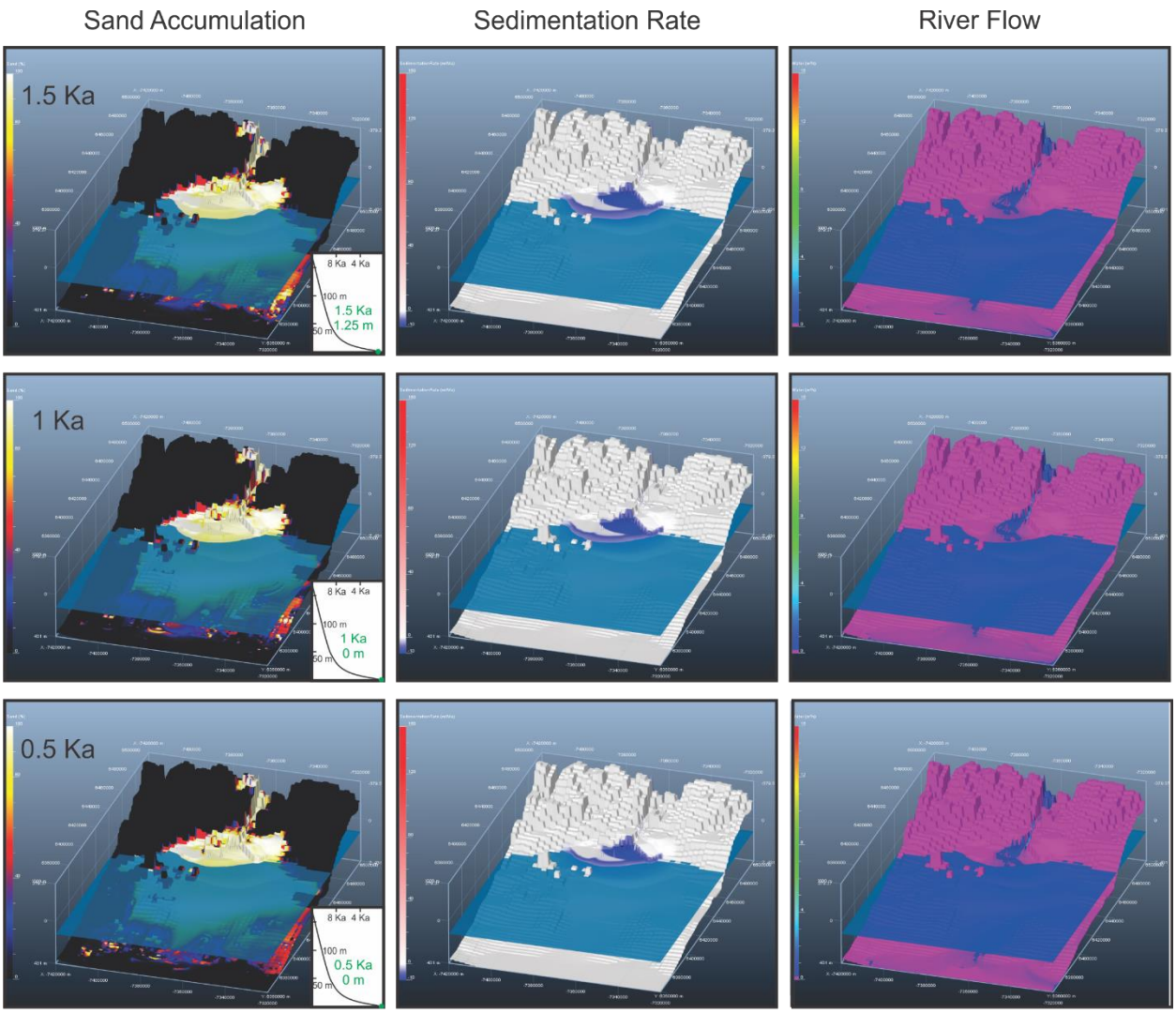

Figure 18: 3D view of Model 1 from 1.5 ka BP to 0.5 ka BP.

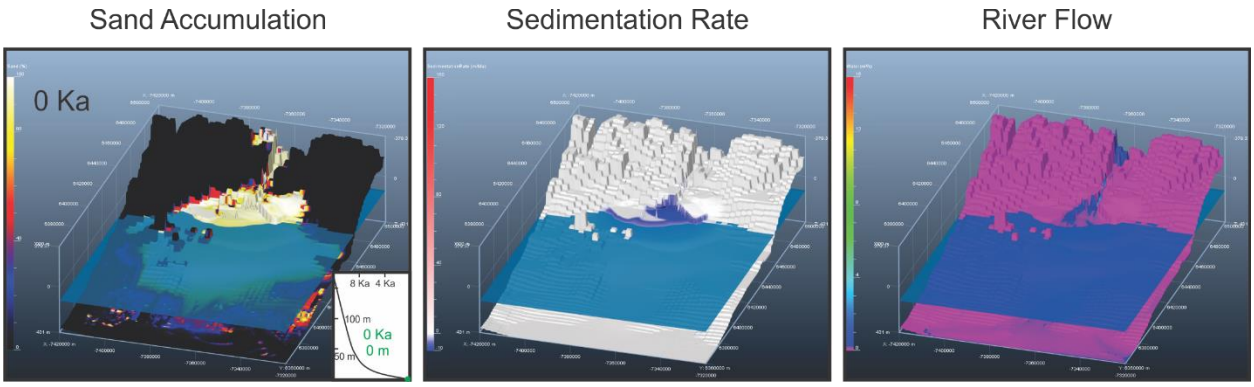

Figure 19: 3D view of Model 1 at present day.

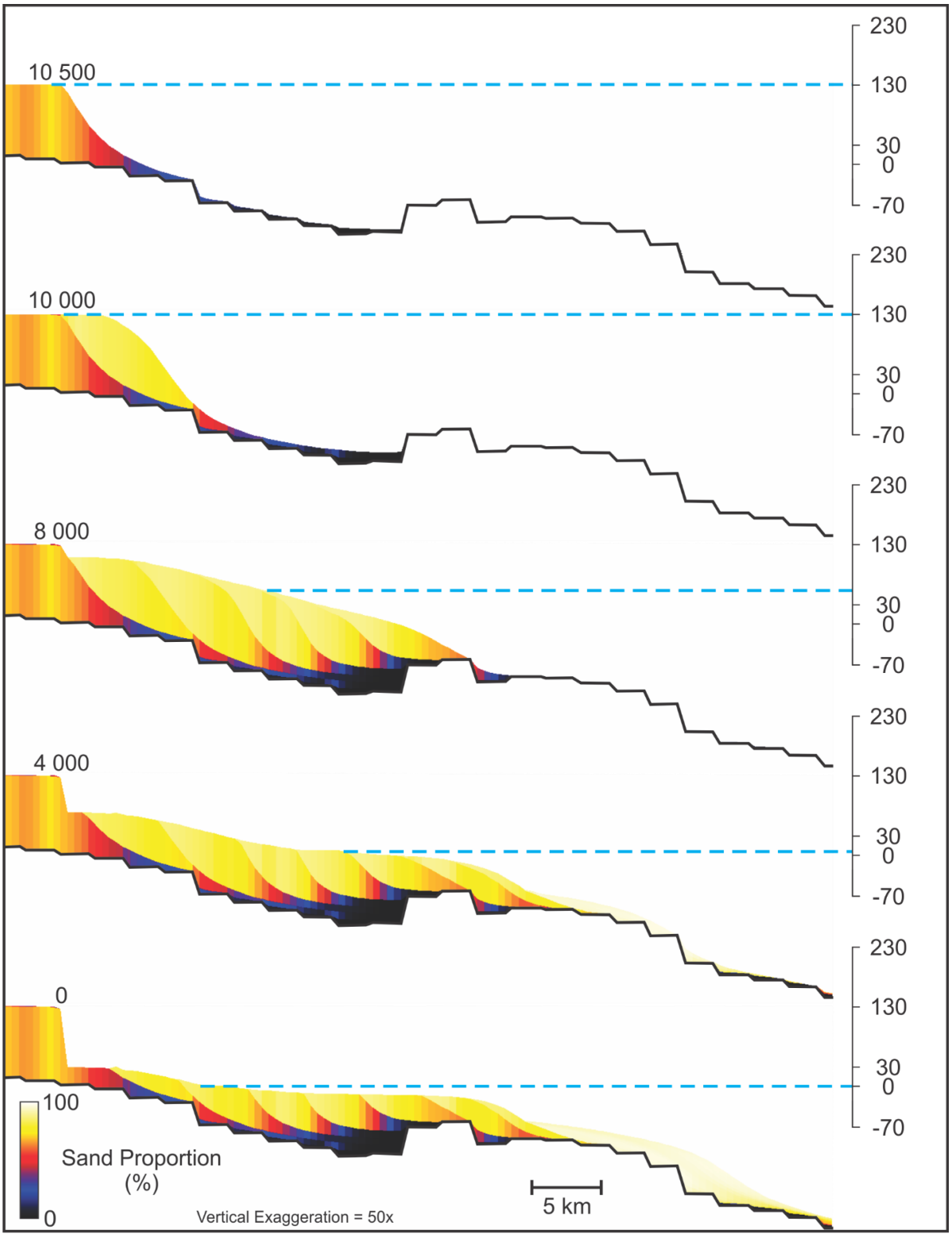

Figure 20:2D cross section of the model 1 delta at various time steps.

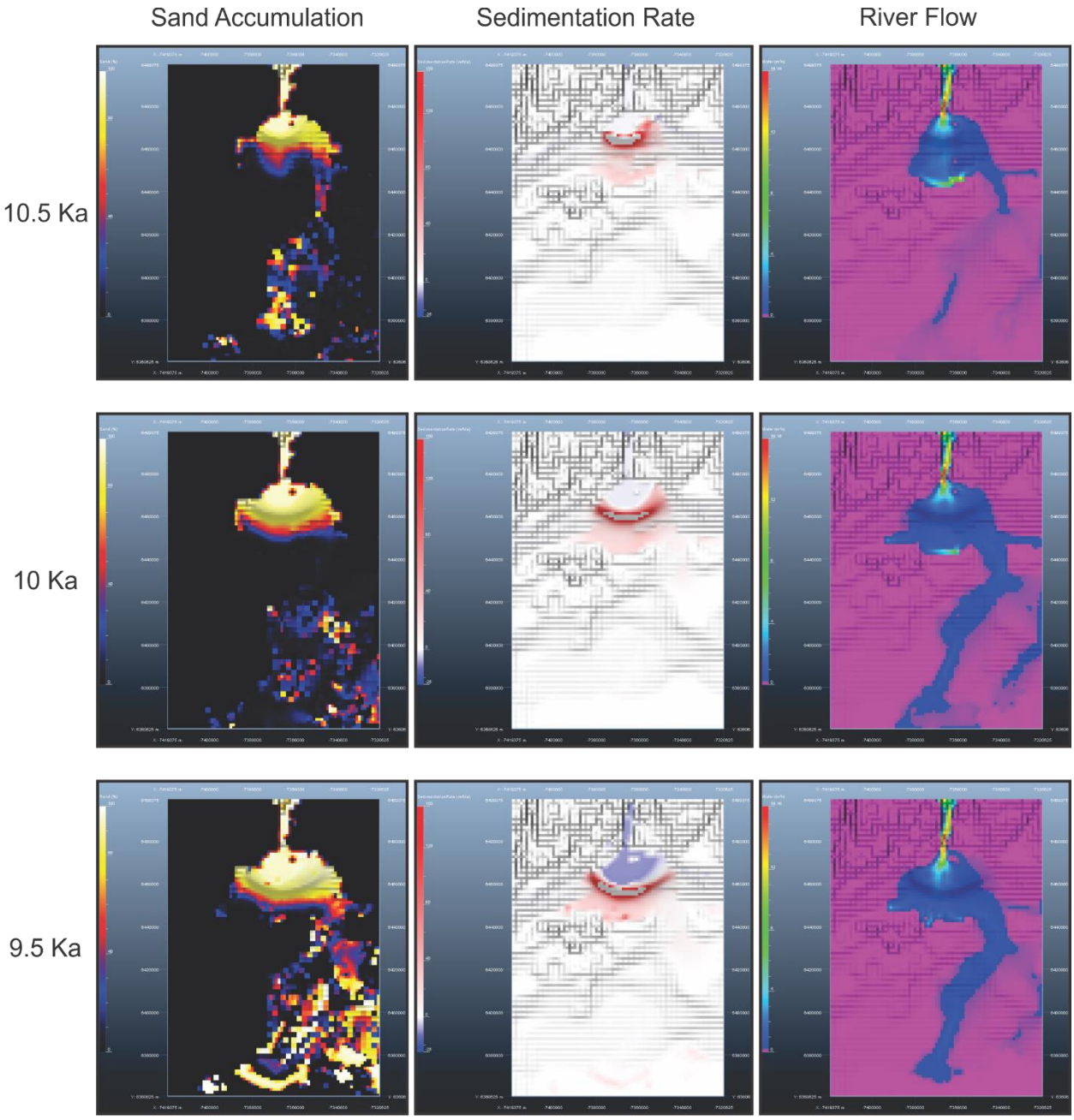

Figure 21: Plan view of delta progradation for Model 2 from 10.5 ka BP to 9.5 ka BP.

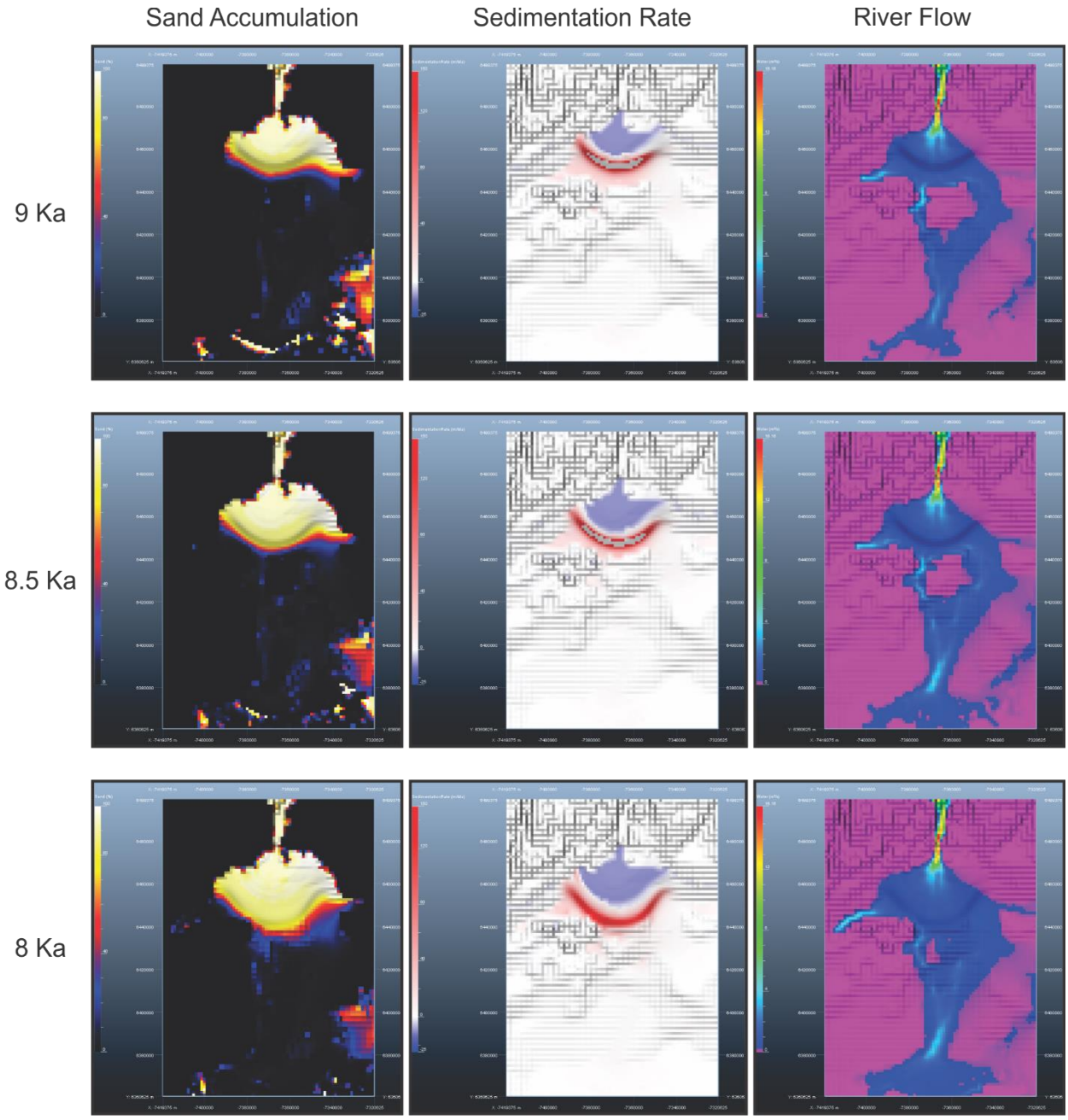

Figure 22: Plan view of delta progradation for Model 2 from 9 ka BP to 8 ka BP.

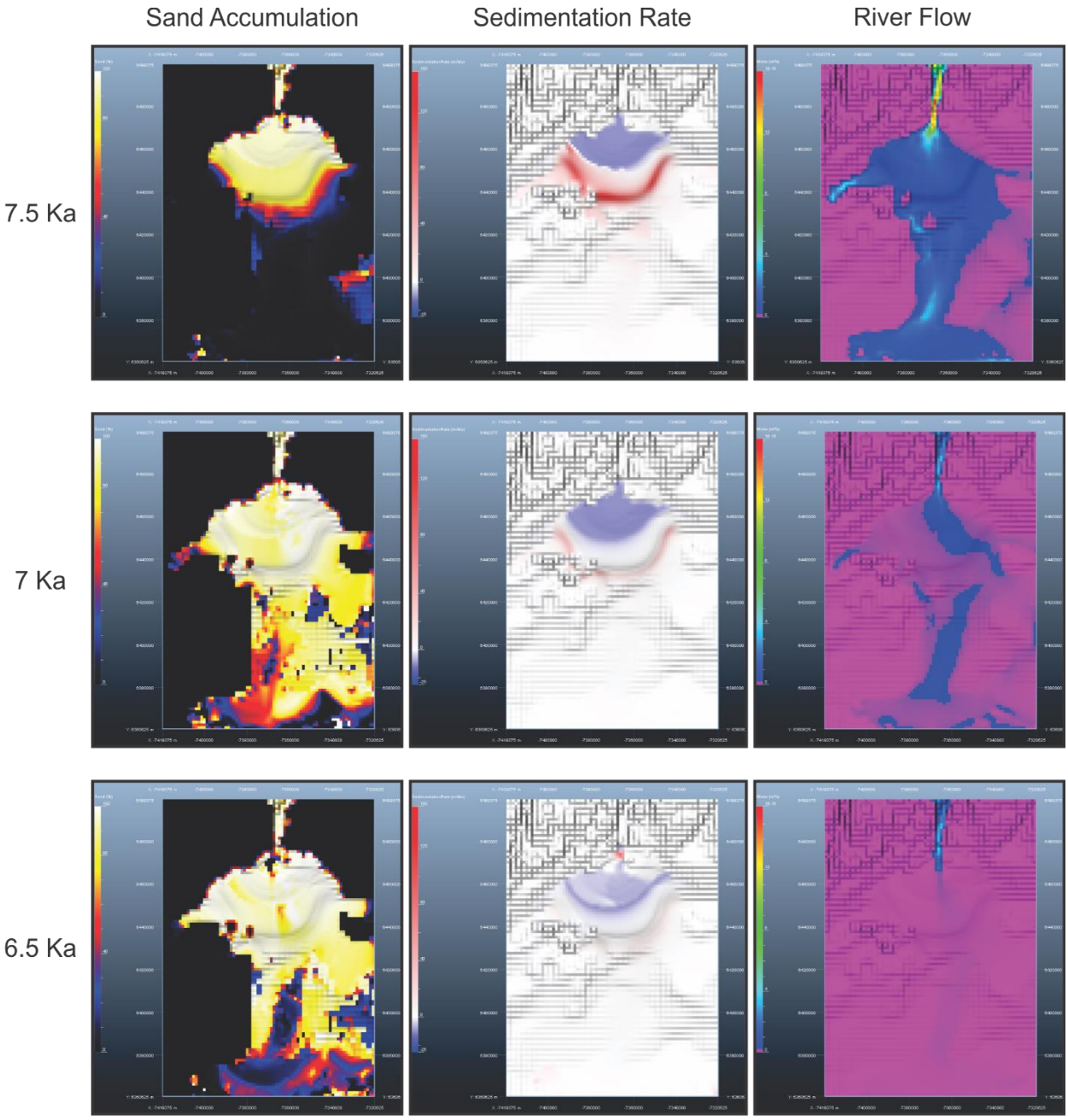

Figure 23: Plan view of delta progradation for Model 2 from 7.5 ka BP to 6.5 ka BP.

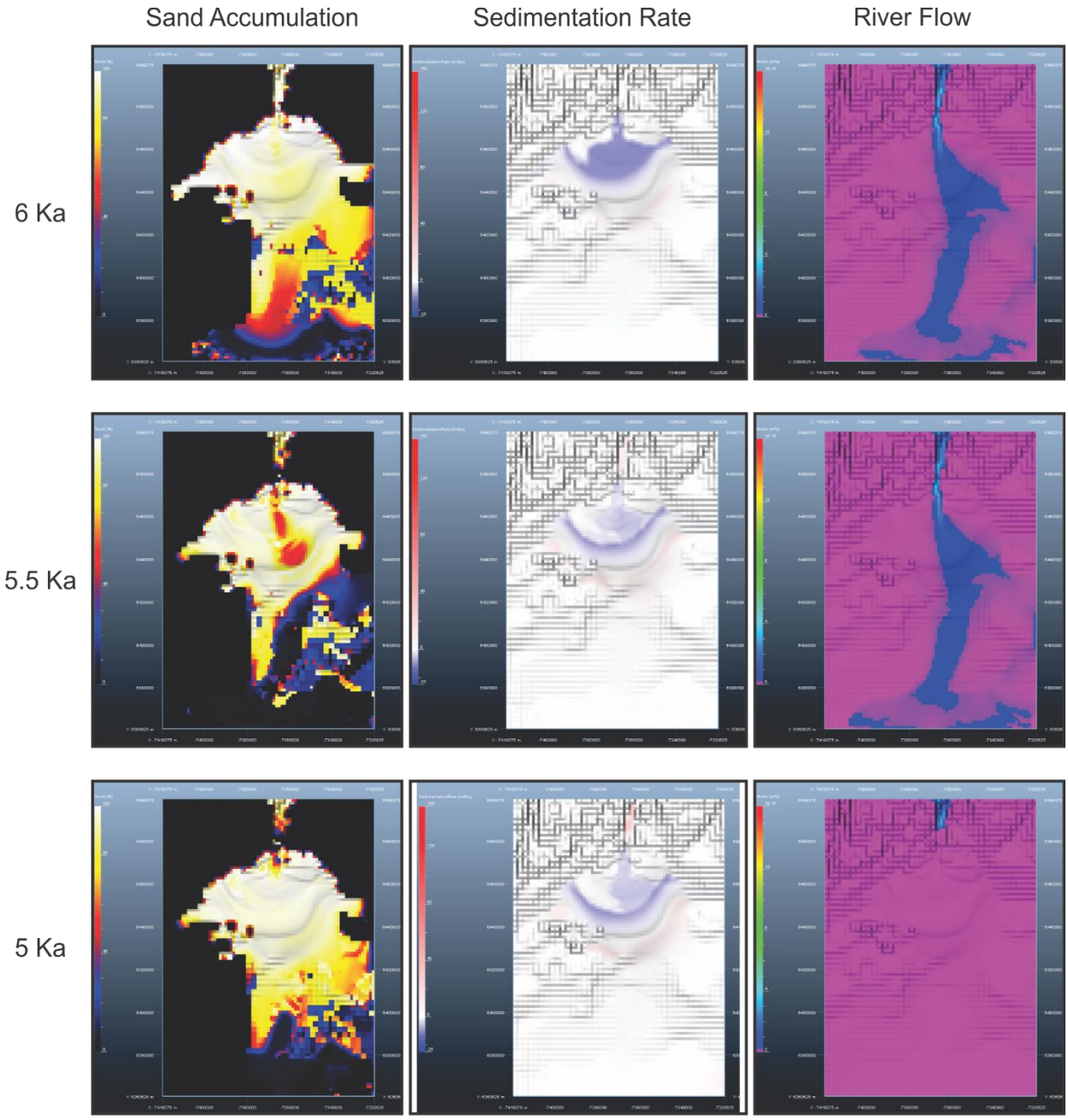

Figure 24: Plan view of delta progradation for Model 2 from 6 ka BP to 5 ka BP.

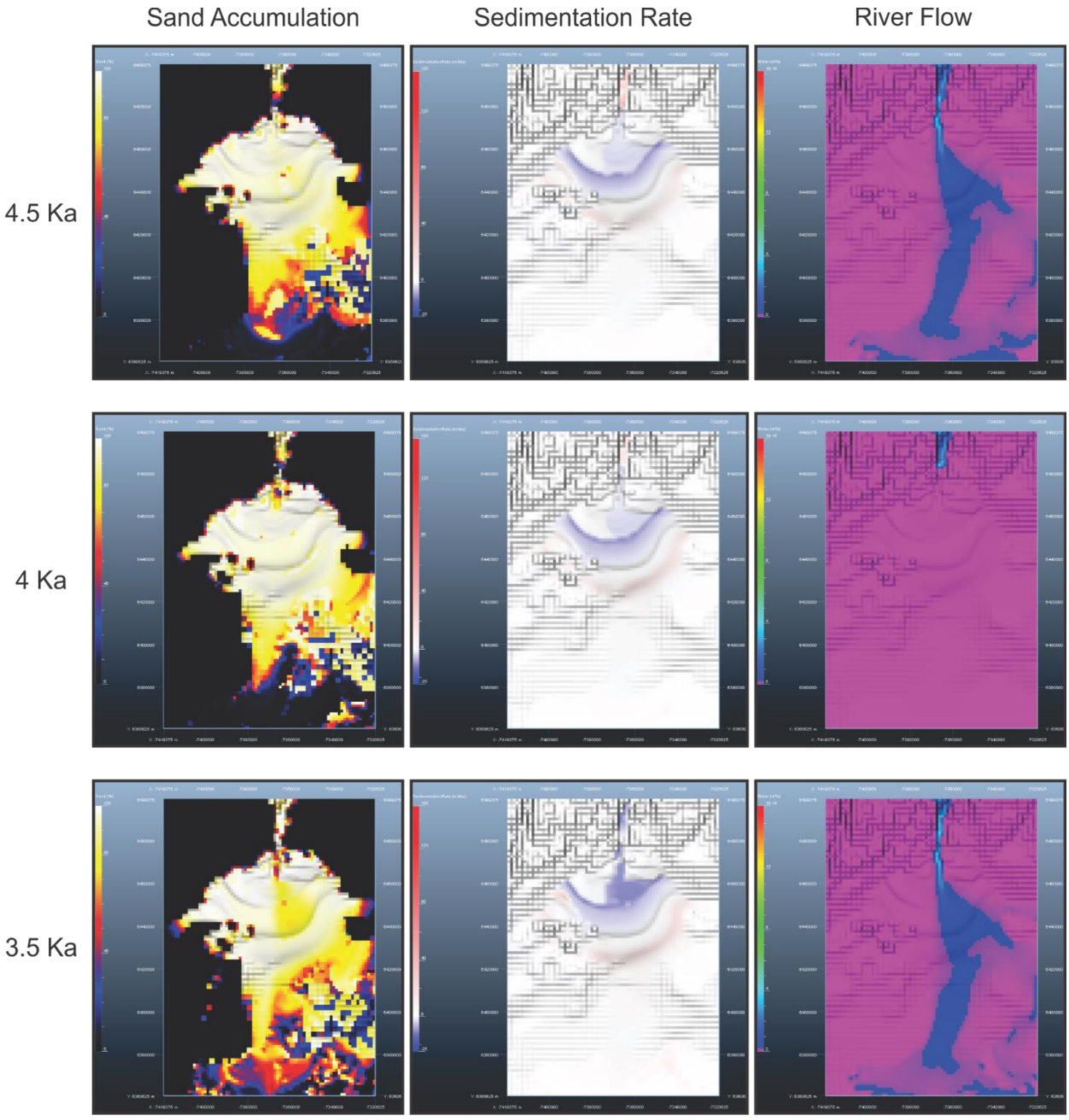

Figure 25: Plan view of delta progradation for Model 2 from 4.5 ka BP to 3.5 ka BP.

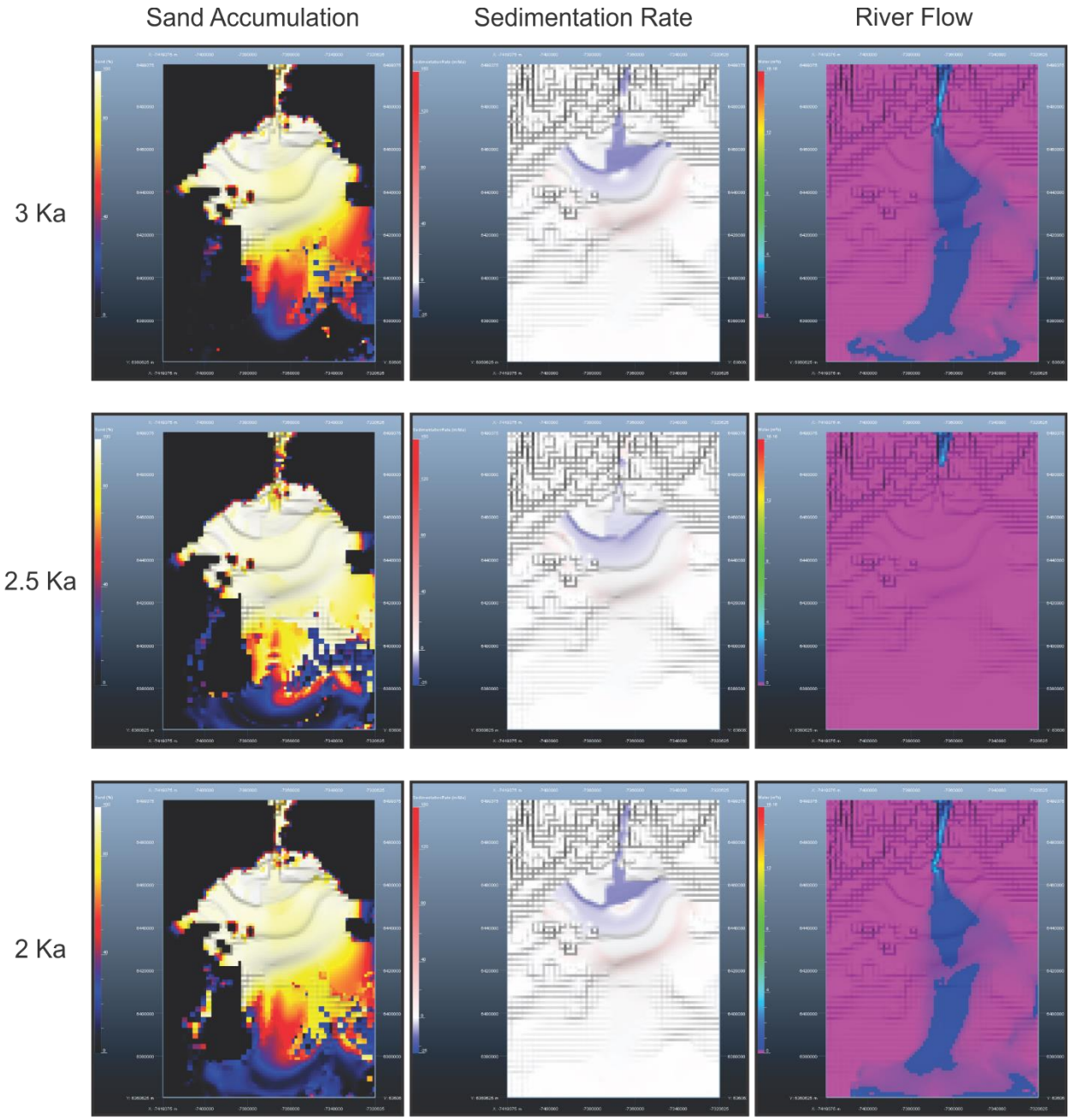

Figure 26: Plan view of delta progradation for Model 2 from 3 ka BP to 2 ka BP.

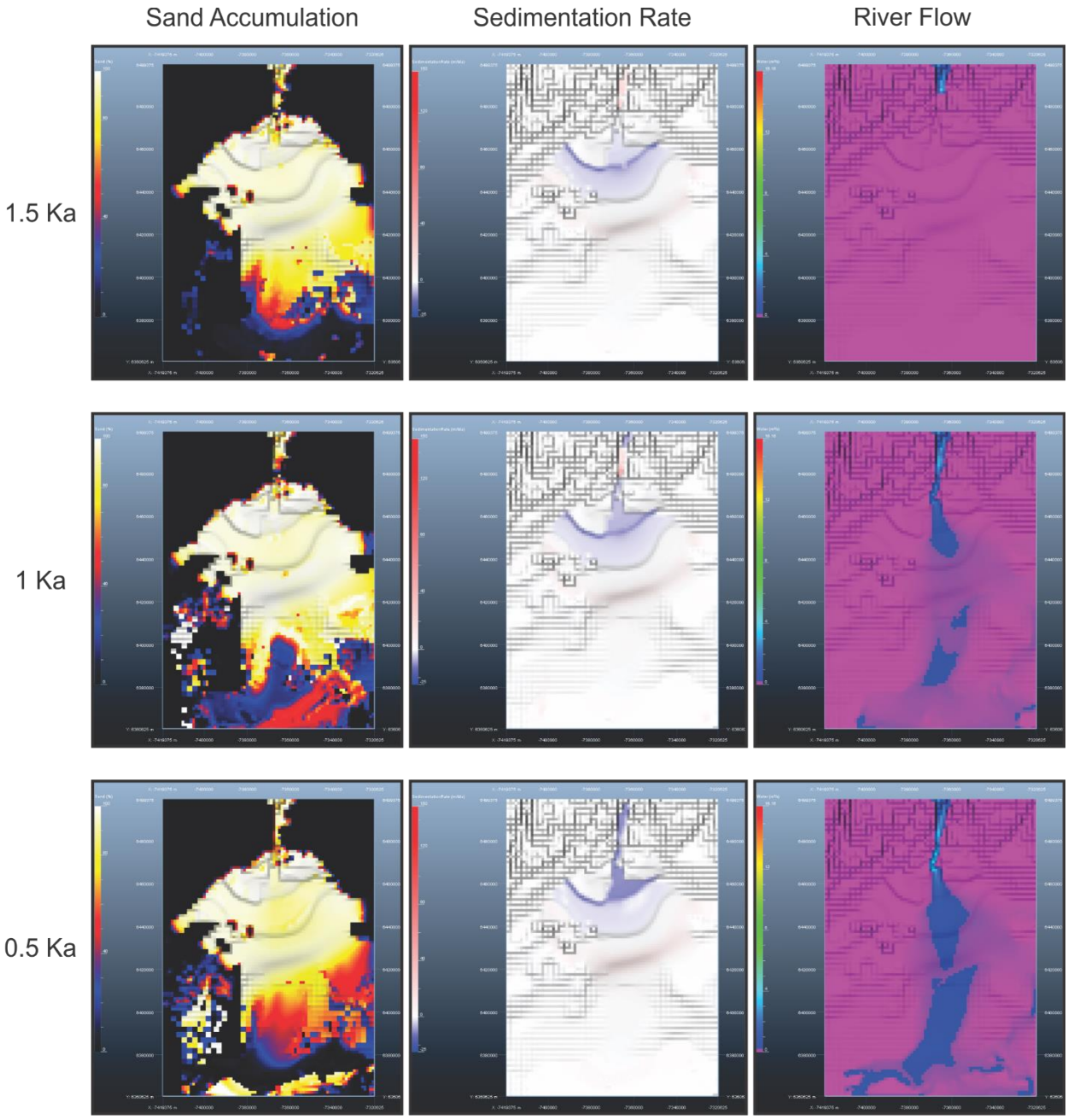

Figure 27: Plan view of delta progradation for Model 2 from 1.5 ka BP to 0.5 ka BP.

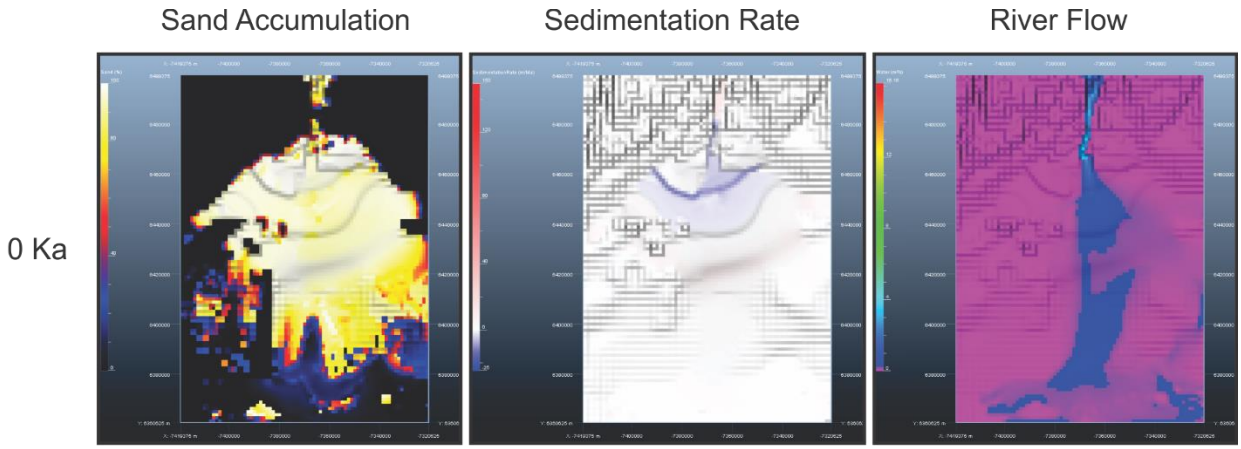

Figure 28: Plan view of delta progradation for Model 2 at present day.

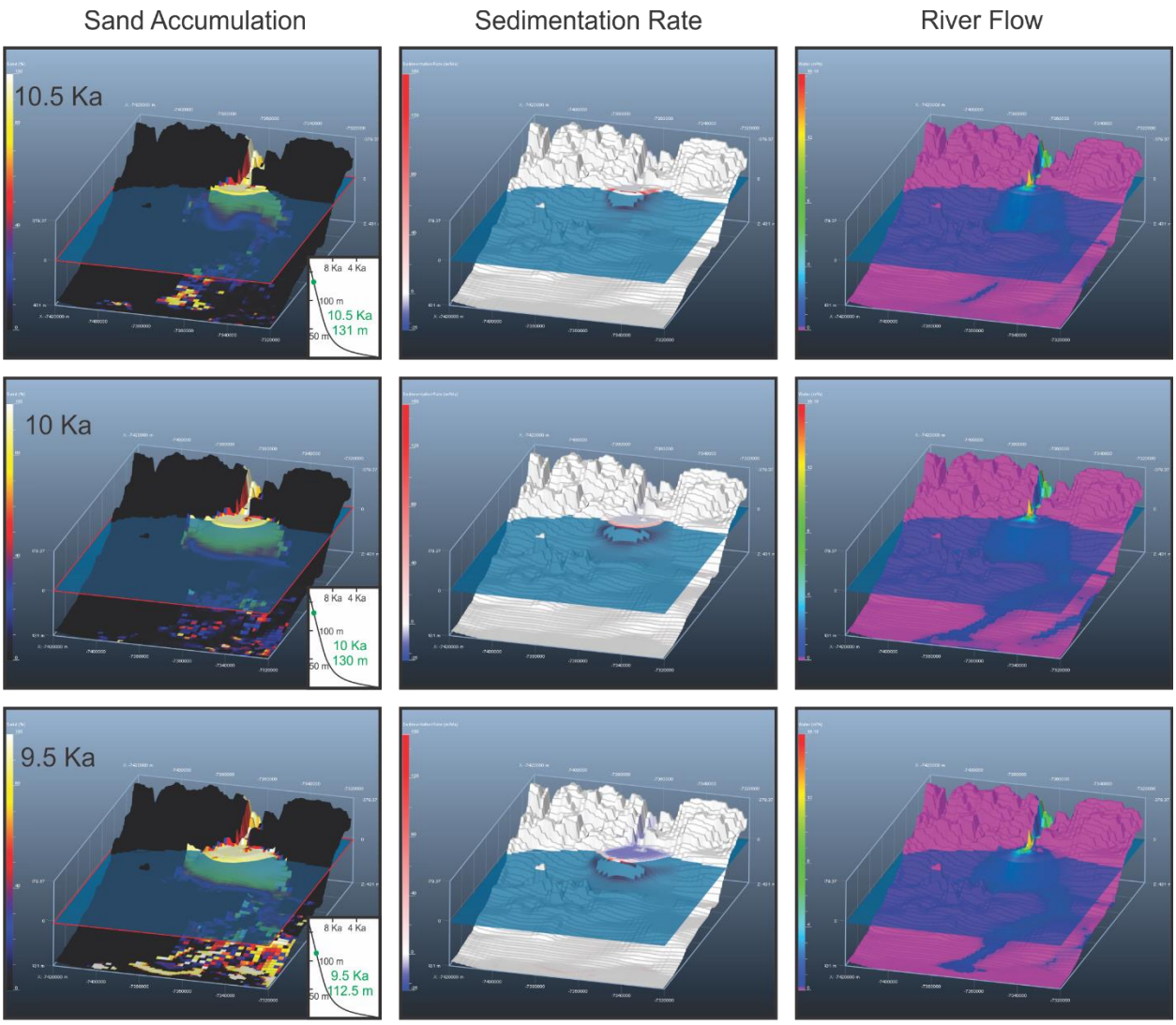

Figure 29: 3D view of model 2 from 10.5 ka BP to 9.5 ka BP.

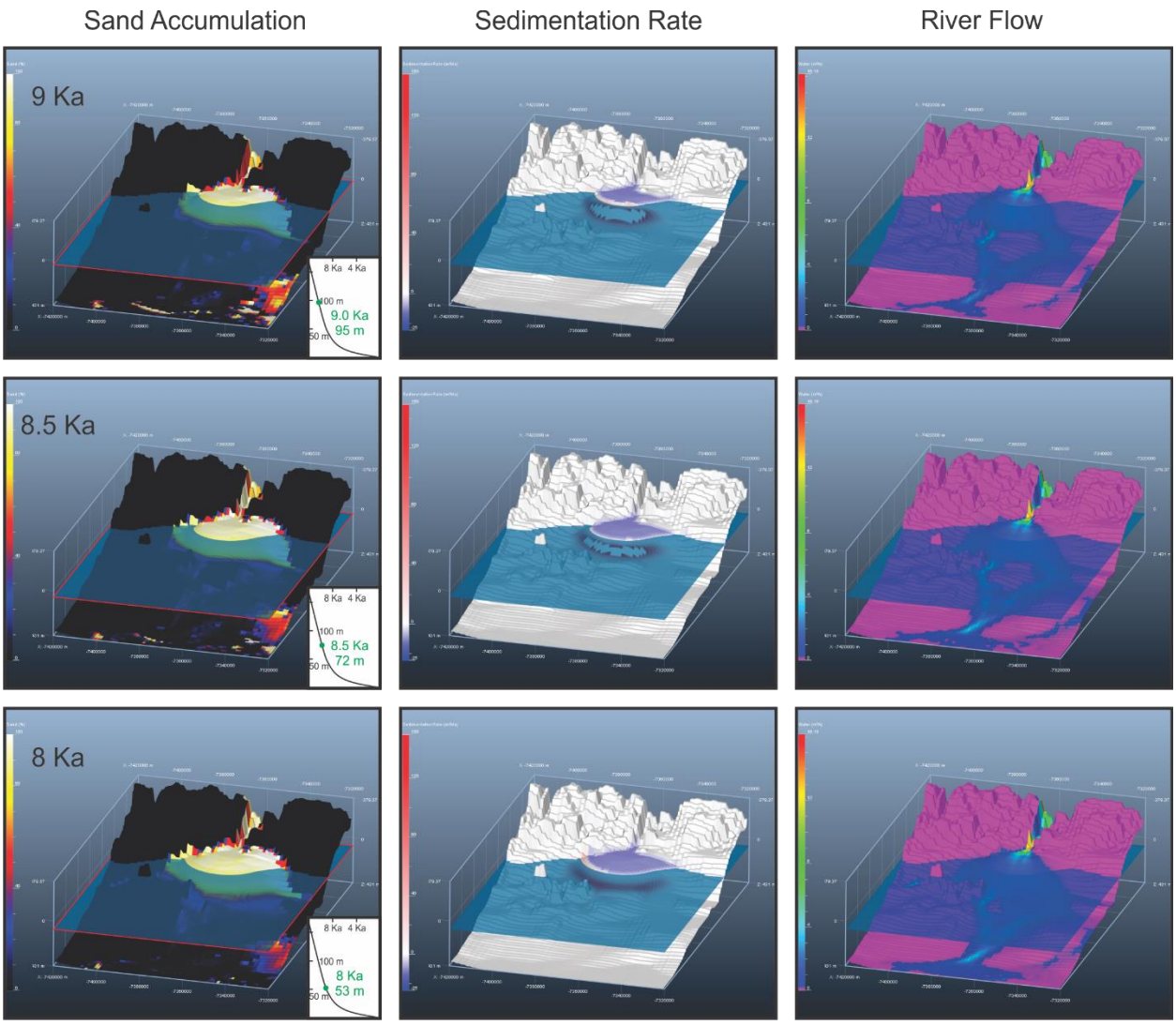

Figure 30: 3D view of model 2 from 9 ka BP to 8 ka BP.

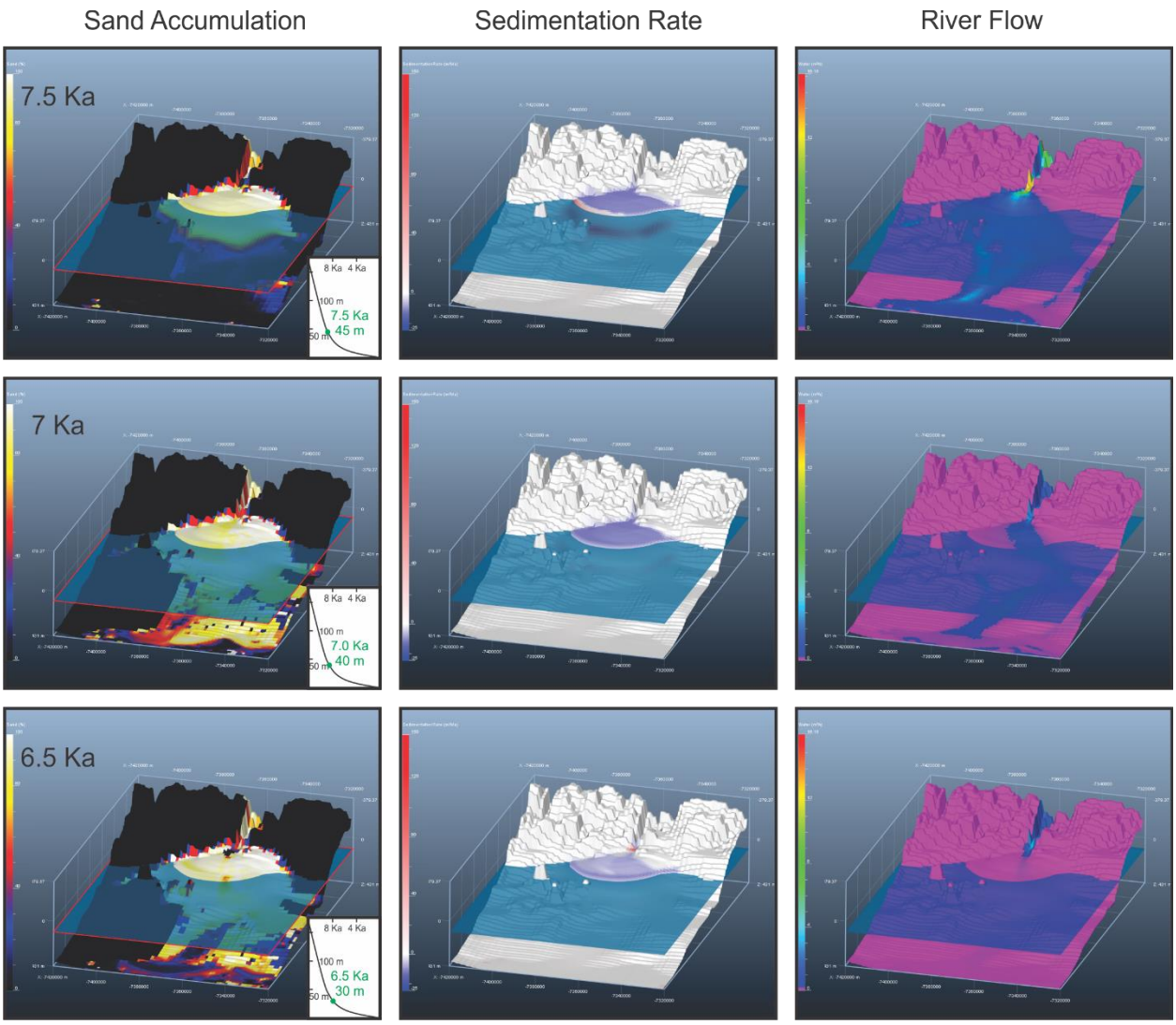

Figure 31: 3D view of model 2 from 7.5 ka BP to 6.5 ka BP.

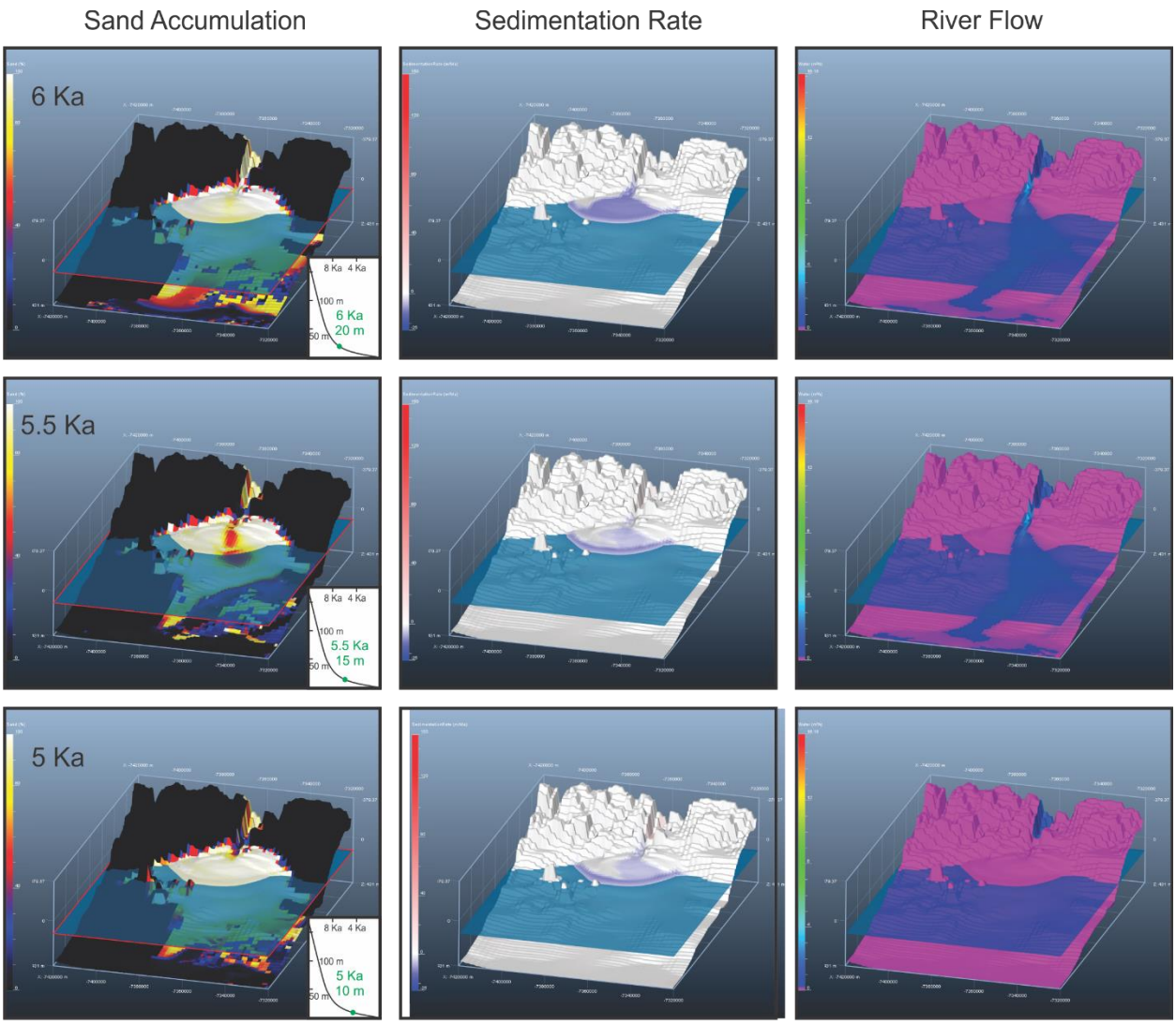

Figure 32: 3D view of model 2 from 6 ka BP to 5 ka BP.

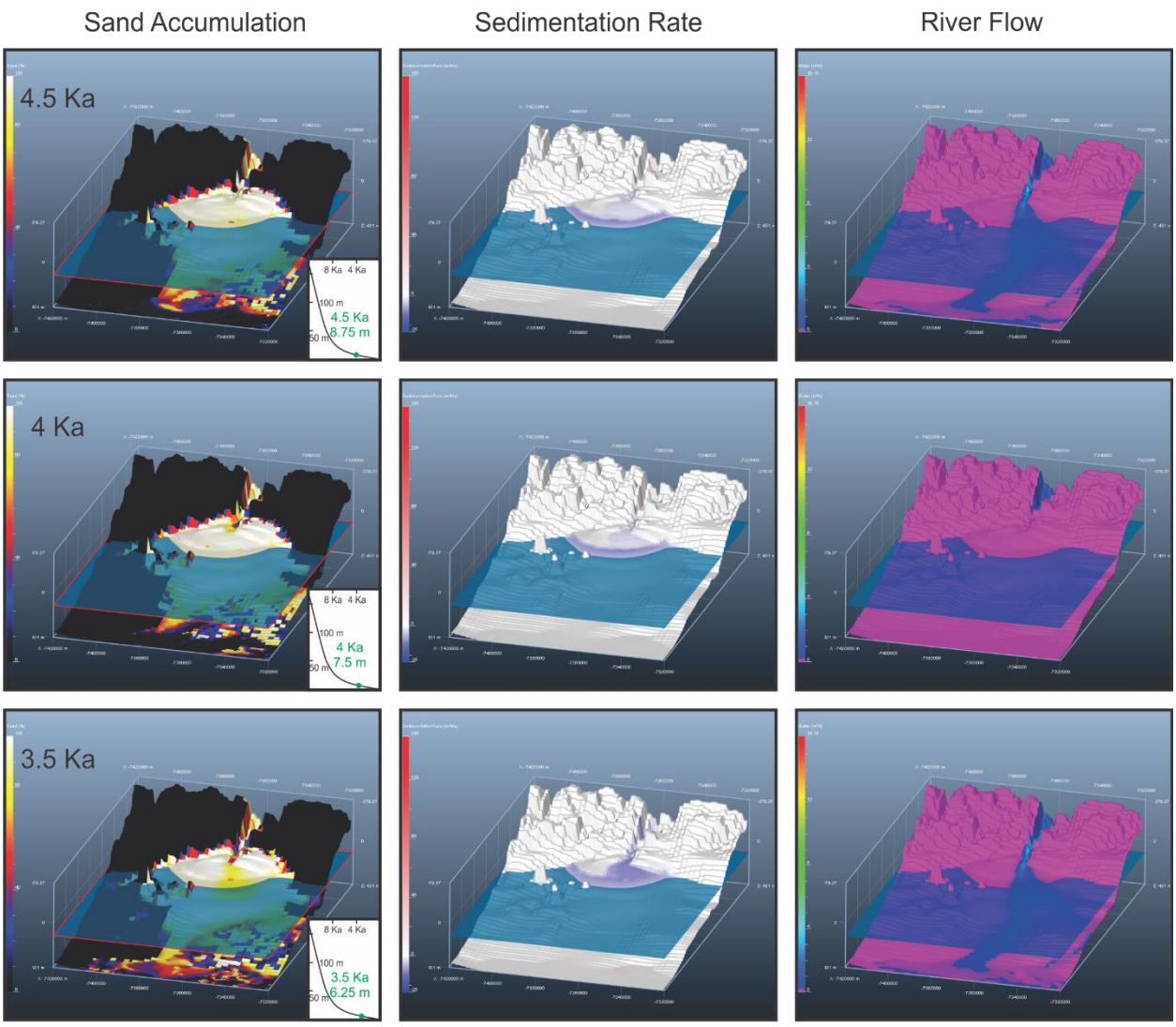

Figure 33: 3D view of model 2 from 4.5 ka BP to 3.5 ka BP.

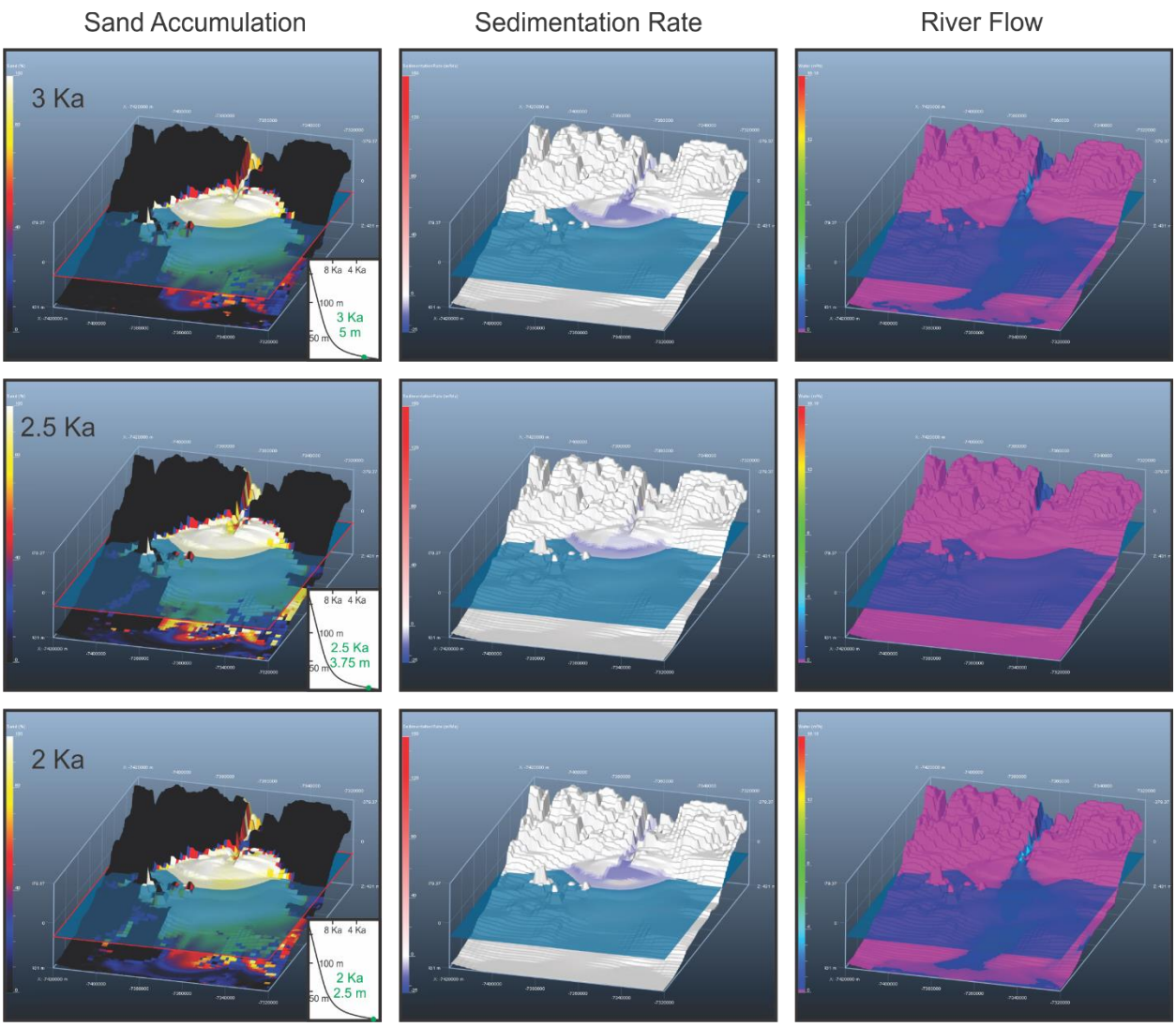

Figure 34: 3D view of model 2 from 3 ka BP to 2 ka BP.

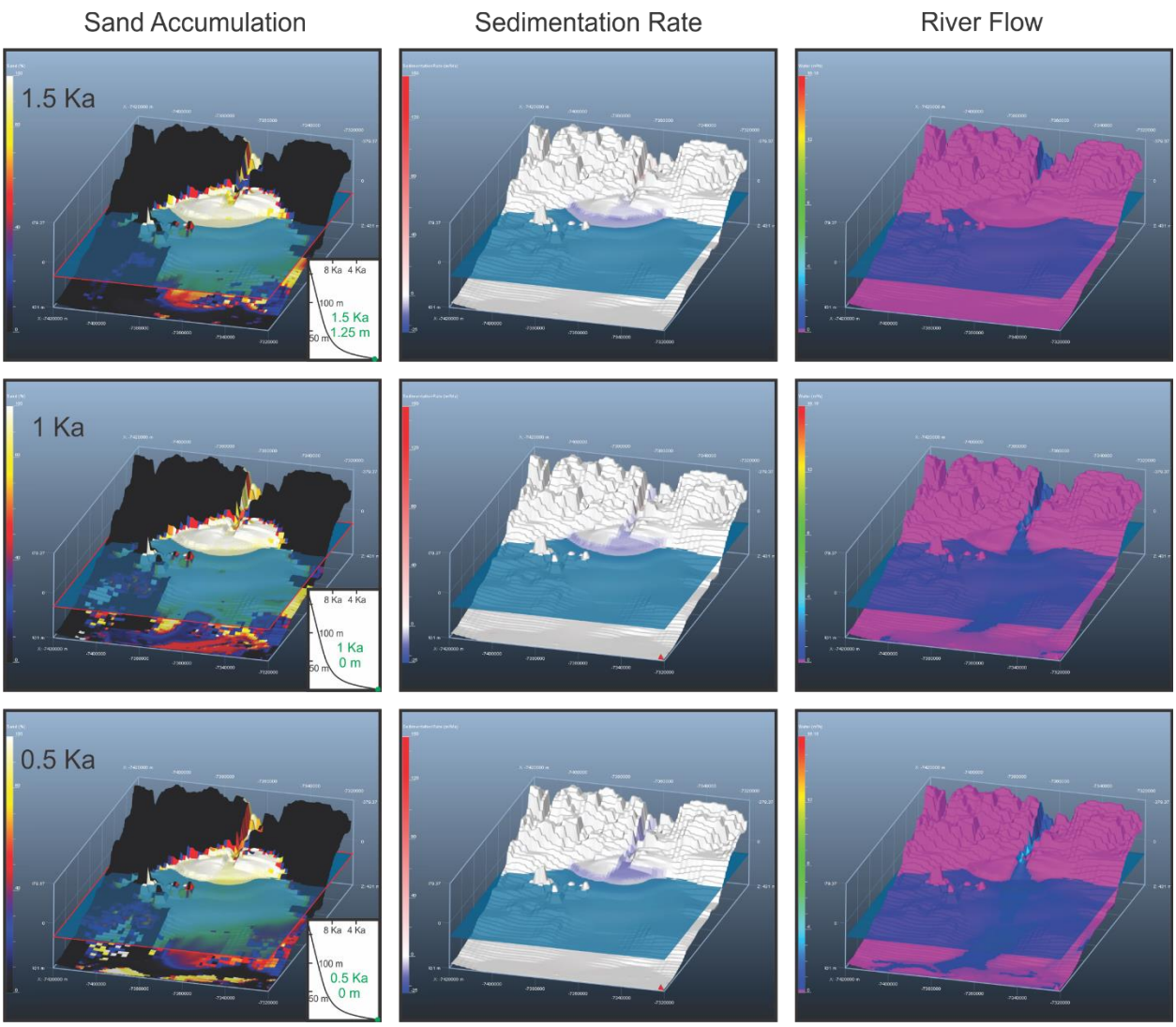

Figure 35: 3D view of model 2 from 1.5 ka BP to 0.5 ka BP.

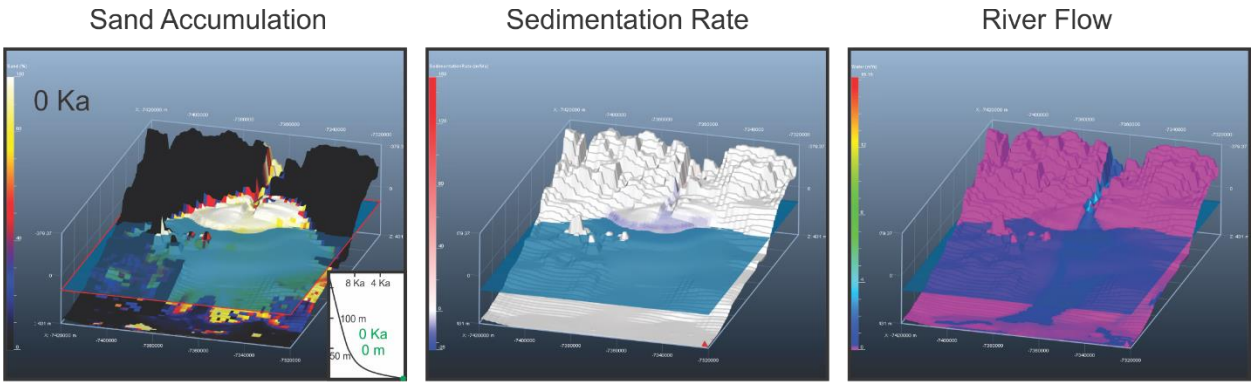

Figure 36: 3D view of model 2 at present day.

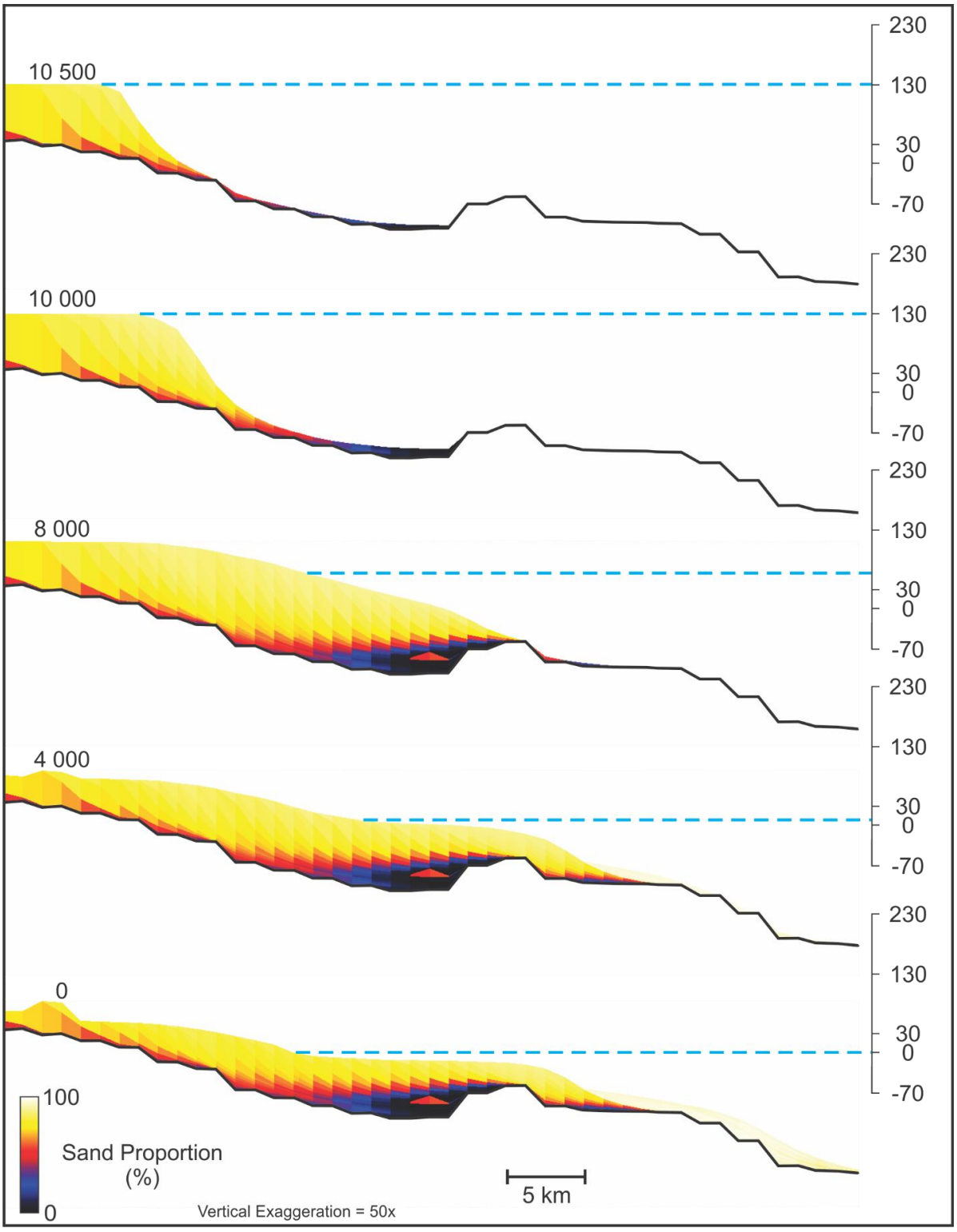

Figure 37: 2D cross section of the Model 2 delta at various time steps.

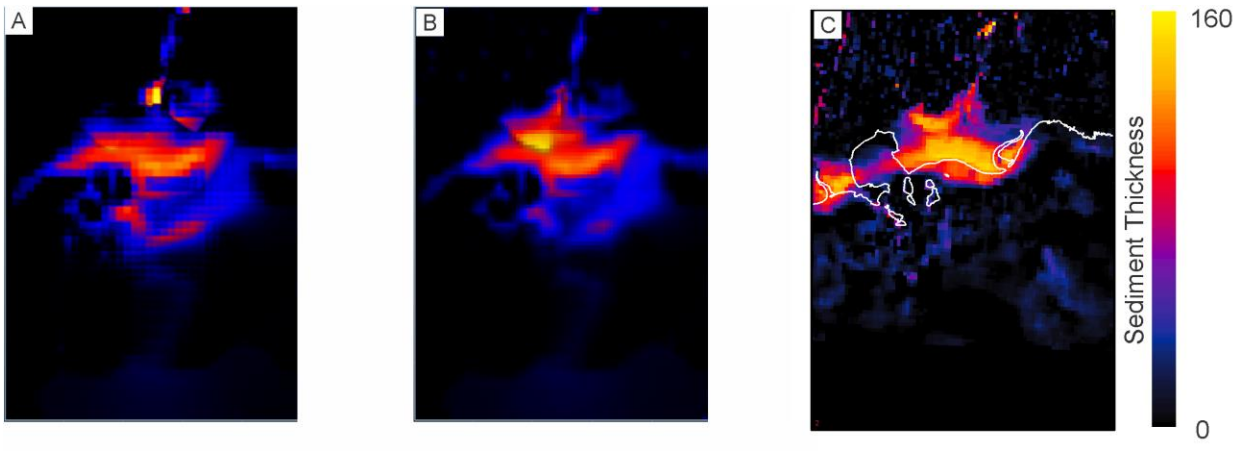

Figure 38: Thickness maps of model 1 (A), model 2 (B), and present-day delta (C).

Table 1: Summary of values used in the Sediment Supply Editor in Model 1

Age (Ma)	11	10	9	8	7.3	5	0
Total Sediment Supply (km^3/Ma)	35	35	35	35	2	2	2
Total Fluvial Discharge (m^3/s)	20	20	20	20	5	5	5

Table 2: Summary of values used in the Transport Editor Used in Model 1

	$K_{gravity\ continental}$	$K_{gravity\ marine}$	$K_{water\ continental}$	$K_{water\ marine}$	K_{wave}	*Critical Slope Failure*	*Maximum Weathering Rate*
Bedrock	0.0000	0.0010	300.0000	8.1791	0.1000	100.0000	0.0000
Sand	0.0000	0.0010	500.0000	0.0000	0.4000	800.0000	10.0000
Clay	0.0000	0.0500	5000.0000	0.0000	1.5000	1500.0000	10.0000

Table 3: Summary of values used in the Sediment Supply Editor in Model 2

Age (Ma)	*11*	*10*	*9*	*8*	*7.3*	*5*	*0*
Total Sediment Supply (km^3/Ma)	35	35	35	35	2	2	2
Total Fluvial Discharge (m^3/s)	25	25	25	25	5	5	5

Table 4: Summary of values used in the Transport Editor Used in Model 2

	$K_{gravity}$ *continental*	$K_{gravity}$ *marine*	K_{water} *continental*	K_{water} *marine*	K_{wave}	*Critical Slope Failure*	*Maximum Weathering Rate*
Bedrock	36.4095	1.1153	300.0000	8.1791	30.0000	100.0000	100.0000
Sand	0.0000	0.0010	500.0000	0.0000	0.4000	800.0000	10.0000
Clay	0.0000	0.0500	5000.0000	0.0000	1.5000	1500.0000	10.0000